ISSN: 0078-415X

Institute of Polar Studies
Report No. 84

A Non-steady Ice-sheet Model Incorporating Longitudinal Stresses

by

Richard B. Alley

Institute of Polar Studies
and
Department of Geology and Mineralogy

1984

OSU

The Ohio State University
Institute of Polar Studies
Columbus, Ohio 43210

Institute of Polar Studies

Report No. 84

A Non-steady Ice Sheet Model Incorporating Longitudinal Stresses: Application to the Adjustment of Interior Regions of an Ice Sheet to Changes in Sea Level

by

Richard B. Alley

Institute of Polar Studies
and
Department of Geology and Mineralogy

1984

Institute of Polar Studies
The Ohio State University
Columbus, Ohio 43210

Richard B. Alley's current address is Geophysical and Polar Research Center, University of Wisconsin at Madison, Madison, Wisconsin 53706.

Copies of this and other publications of the Institute of Polar Studies are available from:

Institute of Polar Studies
The Ohio State University
125 South Oval Mall
Columbus, Ohio 43210
Telephone: 614-422-6531

ABSTRACT

In order to study the effect of sea-level changes on inland ice sheets, a new ice-flow model has been developed that explicitly includes longitudinal stresses. Two-dimensional flow is assumed, and the flow-law parameter and longitudinal-deviatoric stress are taken to be weighted averages over depth. The flow-law equations for longitudinal and shear deformation are then averaged over thickness. The resulting equations, together with continuity and a bottom-sliding relation, form a simple one-dimensional system of equations that describes changes in ice-sheet configuration over time.

Sea-level rise causes a wave of thinning to propagate upglacier in an ice sheet with terminal position controlled by sea level. The wave of thinning slows, diffuses, and is damped as it moves upglacier; thus, perturbations near the coast must be large and be long lasting to affect inland regions.

Model calculations show that post-Wisconsinan sea-level rise has caused 110 m thinning at Dome C, East Antarctica, and that response is now 70 percent complete. Accumulation rate probably increased at the same time, however, and including this in the model reduces calculated thinning. For a 10 percent increase in accumulation rate from Wisconsinan to Holocene, there has been 75 m post-Wisconsinan thinning due to combined effects of sea-level rise and accumulation-rate increase.

ACKNOWLEDGEMENTS

I would like to thank those people whose contributions made this study possible. The Master's Examination Committee, consisting of Professors C. B. B. Bull, G. D. McKenzie, and R. R. B. von Frese, provided helpful suggestions. Dr. John Bolzan gave me many insights into physical processes, and supplied important preliminary data from his studies at Dome C. My wife, Cindy, provided much-needed support. I am especially grateful to my adviser, Dr. Ian Whillans, who supplied guidance throughout this project, and who helped me to see beyond the immediate problem and consider the larger issues of the science.

This work was supported by National Science Foundation grant DPP-7920824A02 to The Ohio State University Research Foundation and to Dr. Ian Whillans, Institute of Polar Studies and Department of Geology and Mineralogy.

TABLE OF CONTENTS

LIST OF FIGURES

LIST OF TABLES

LIST OF SYMBOLS

Parameters. Many of these parameters take subscripts or superjacent modifiers, which are listed below.

A.....flow-law parameter

$\bar{b}$.....accumulation rate

Δ.....change in following variable. Δh and ΔH are changes in thickness over the course of an experiment. $\Delta \bar{b}$ is change in accumulation rate at beginning of experiment. Other uses represent step length in finite-difference calculation or change in parameter over that step.

Δt_t....time required for sea level to rise

$\dot{\varepsilon}$ .....strain rate

$f_i( )$..some function of the variables listed in parantheses

g.....acceleration caused by gravity

h.....ice-sheet thickness

$\dot{h}$.....time-rate of change of ice-sheet thickness

H.....ice-sheet thickness at the ice divide

L.....ice-sheet half-width

m.....exponent in power-law estimate of flow-law parameter as a function of depth

p.....constant in expression for ice-sheet response time

ρ .....density of ice, assumed constant

σ' .....longitudinal-deviatoric stress

t.....time

T.....temperature

θ .....ice-sheet response time

τ.....shear stress

τ_e.....total effective stress

u.....horizontal component of ice velocity

w.....magnitude of vertical component of ice velocity

x.....coordinate axis on the horizontal bed in the direction of ice flow

z.....coordinate axis perpendicular to the bed

Subscripts and superjacent modifiers.
All subscripts refer to preceding parameter.

$(_o)$....value at the origin, chosen 300 km upglacier from the grounding line of an ice stream (h,u). Also, value at the bed (A)

$(_1)$....(with $\bar{A}$) weighted average over thickness of flow-law parameter obtained from the shear flow law

$(_2)$....(with $\bar{A}$) weighted average over thickness of flow-law parameter obtained from longitudinal flow law

$(_b)$....value at the bed

$(_d)$....value caused by internal deformation

(e)....equilibrium or steady-state value

$(_i)$....counter for finite-difference calculations

$(_j)$....counter for finite-difference calculations

$(_m)$....maximum value

$(_s)$....surface value

$(_t)$....typical value

$(_w)$....Wisconsinan-maximum value

$(_x)$....component in the x direction

$(_{xz})$...component in the x direction along a plane perpendicular to the z axis

$(_z)$....component in the z direction

$(\bar{})$....average through thickness of the subjacent parameter. Average is weighted in the case of σ' and A, and is simple in other cases.

Math symbols.

∂.....partial derivative

∂^2.....second partial derivative

exp....base of the Napieran logarithm, e, raised to the following power.

Σ .....summation

$\gg$ .....greater than. Repetition indicates much greater than

$\ll$ .....less than. Repetition indicates much less than

$\sim$ .....is approximately equal to

INTRODUCTION

The lateral extent of the East Antarctic ice sheet is controlled largely by sea level. During the Pleistocene low-stand, the ice sheet was able to advance 75 to 90 km to the edge of the continental shelf (Hollin, 1962). Holocene sea-level rise caused grounding-line retreat to the present position and ice-sheet thinning.

Grounding-line retreat reduces bed area and thus reduces backstress from the bed on grounded ice upglacier; near-coastal thinning increases surface slope and also shear stress at the upglacier end of the thinning region. Both increased shear stress and, to a lesser extent, reduced backstress lead to increased strain rate and thinning a short distance upglacier. Sea-level rise thus causes a wave of thinning to propagate upglacier.

To study this wave of thinning, a simple, nonsteady ice-flow model has been developed incorporating both longitudinal and shear stresses for two-dimensional flow over a horizontal bed. The flow-law equations for longitudinal and for shear deformation are averaged through thickness to obtain two one-dimensional equations for ice flow. These equations, combined with continuity and a bottom-sliding relation, form a system which may be solved numerically to describe ice-sheet response to changes in sea level, accumulation rate, or other parameters.

PHYSICAL CONCEPTS

Consider two-dimensional glacial flow over a horizontal bed, with the origin on the bed under the ice divide, x axis horizontal along a flow line, and z axis vertical. The flow law for polycrystalline ice, with exponent equal to three and horizontal gradients in vertical velocity small (Appendix A) then leads to (Paterson, 1981, p. 89)

$$\frac{\partial u}{\partial x}=A(\sigma_x'^2+\tau_{xz}^2)\sigma_x' \tag{1}$$

$$\frac{\partial u}{\partial z}=2A(\sigma_x'^2+\tau_{xz}^2)\tau_{xz} \tag{2}$$

where u is the horizontal component of ice velocity, σ_x' and τ_{xz} are longitudinal-deviatoric and shear stress, respectively, and the flow-law parameter, A, depends on temperature and other factors (Hooke, 1981).

For flow over a horizontal bed, shear stress varies primarily with ice thickness and surface slope (Budd, 1968; 1970) so that

$$\tau_{xz}=\rho g(h-z)\frac{\partial h}{\partial x} \tag{3}$$

where ρ is density of ice (assumed constant), g is acceleration due to gravity, and h is ice-sheet thickness. This relation is also valid for flow over realistic basal topography, if average thickness and surface slope are used (Budd, 1968; 1970).

In addition to the flow law for polycrystalline ice and the shear stress due to gravity, the concept of mass continuity is used. For

ice of constant density, this may be written

$$\frac{\partial(h\bar{u})}{\partial x}=\dot{b}-\dot{h} \tag{4}$$

where $\dot{b}$ is net accumulation rate, $\dot{h}$ is time-rate of change of ice thickness, and $\bar{u}$ is horizontal velocity averaged over depth.

In the general case, horizontal velocity is due both to deformation within the ice and to bottom sliding. In applying the model to East Antarctica, it is assumed that there is no bottom sliding (Appendix D). The model can be applied to regions where bottom sliding is important, if a bottom-sliding relation is specified.

DERIVATION OF MODEL

The approach followed here is to develop a one-dimensional system of equations describing nonsteady ice flow in terms of ice-sheet configuration, h(x,t). This is accomplished by substituting depth-averaged quantities for some parameters in the flow-law equations (1) and (2), and then explicitly averaging these equations over depth.

The flow-law parameter, A, depends on temperature, fabric development, and other factors (Hooke, 1981), and its depth-dependence is not well-understood. Here it is assumed that

$$A=\bar{A} \tag{5}$$

where $\bar{A}$ is a weighted average of the flow-law parameter over depth which varies only slowly with distance along the x axis (see also Appendix B).

Depth-variation of longitudinal-deviatoric stress, σ'_x, is also not well-understood. Longitudinal-deviatoric stress has been calculated as a function of depth in Appendix C, assuming: 1) Robin-type temperature profile (Robin, 1955; Clarke and others, 1977); 2) Flow-law parameter dependent only on temperature, with temperature-dependence recommended by Paterson (1981, p. 39); and 3) Two-dimensional incompressible flow, with various vertical-strain-rate ($\dot{\varepsilon}_z$) models including $\dot{\varepsilon}_z$ constant and $\dot{\varepsilon}_z$ varying linearly with depth. The results show that σ'_x does vary with depth. In the deep regions of shear-dominated ice sheets and throughout ice streams, where most deformation occurs, longitudinal-deviatoric stress varies more slowly

depth than does shear stress. Thus, it is reasonable to assume that

$$\sigma'_x = \bar{\sigma}'_x \tag{6}$$

where $\bar{\sigma}'_x$ is a weighted average over depth of the longitudinal-deviatoric stress.

Using assumptions (5) and (6), it is now possible to average (1) and (2) over depth to obtain equations that involve functions of x only. These one-dimensional equations may be expressed in terms of the horizontal gradient of horizontal ice flux, so that they are compatible with the continuity equation (4). It should be noted that although the weighting schemes for $\bar{\sigma}'_x$ and $\bar{A}$ from integrating equations (1) and (2) differ, the weighting is quite similar (Appendix B). Errors introduced by ignoring this complication are small.

Integrating the shear flow law (2) from the bed to z yields

$$u(z) = 2\bar{A}\left[\rho g \frac{\partial h}{\partial x}\left(hz - \frac{1}{2}z^2\right)\bar{\sigma}'^2_x + \left(\rho g \frac{\partial h}{\partial x}\right)^3\left(h^3 z - \frac{3}{2}h^2 z^2 + hz^3 - \frac{1}{4}z^4\right)\right] + u_b \tag{7}$$

where u_b is the basal-sliding velocity.

Integrating (7) over thickness yields

$$h\bar{u} = 2\bar{A}\left[\frac{1}{3}\rho g h^3 \frac{\partial h}{\partial x}\bar{\sigma}'^2_x + \frac{1}{5}\left(\rho g \frac{\partial h}{\partial x}\right)^3 h^5\right] + h u_b \tag{8}$$

and differentiating with respect to x

$$\frac{\partial(h\bar{u})}{\partial x} = \bar{A}\left\{\bar{\sigma}'^2_x\left[\frac{2}{3}\rho g h^3 \frac{\partial^2 h}{\partial x^2} + 2\rho g\left(h\frac{\partial h}{\partial x}\right)^2\right] + \bar{\sigma}'_x\left[\frac{4}{3}\rho g h^3 \frac{\partial h}{\partial x}\frac{\partial \bar{\sigma}'_x}{\partial x}\right]\right.$$

$$\left. + (\rho g)^3 h^4 \left(\frac{\partial h}{\partial x}\right)^2\left[2\left(\frac{\partial h}{\partial x}\right)^2 + \frac{6}{5}h\frac{\partial^2 h}{\partial x^2}\right]\right\} + \frac{\partial(h u_b)}{\partial x} \quad . \tag{9}$$

Integrating the longitudinal flow law (1) through thickness

$$\int_o^h \frac{\partial u}{\partial x} dz = \bar{A} h [\bar{\sigma}_x'^3 + \frac{1}{3} \bar{\sigma}_x' (\rho g h \frac{\partial h}{\partial x})^2] \tag{10}$$

and changing the order of integration and differentiation on the left-hand side

$$\frac{\partial}{\partial x}(\int_o^h u dz) - u(h) \frac{\partial h}{\partial x} = \bar{A} h [\bar{\sigma}_x'^3 + \frac{1}{3} \bar{\sigma}_x' (\rho g h \frac{\partial h}{\partial x})^2] \tag{11}$$

The first term on the left-hand side of (11) is the horizontal gradient of horizontal ice flux, which is to be used in the equation of continuity (4). The second term is evaluated from (7) by setting z equal to h. Hence

$$\frac{\partial (h\bar{u})}{\partial x} = \bar{A} h [\bar{\sigma}_x'^3 + \rho g h (\frac{\partial h}{\partial x}) \bar{\sigma}_x'^2 + \frac{1}{3} (\rho g h \frac{\partial h}{\partial x})^2 \bar{\sigma}_x' + \frac{1}{2} (\rho g h)^3 (\frac{\partial h}{\partial x})^4] + u_b \frac{\partial h}{\partial x} \tag{12}$$

Equations (9) and (12) are one-dimensional restatements of the flow-law equations (1) and (2). They are combined to form equation (13) below, eliminating the horizontal gradient in horizontal ice flux. Equation (13) can be solved for depth-averaged longitudinal-deviatoric stress, which can be used in either (9) or (12) to calculate the horizontal gradient in horizontal ice flux. This in

turn can be applied in the equation of continuity. Thus, the equations

$$0=\bar{\sigma}_x'^3-\bar{\sigma}_x'^2(\rho gh)\left[\left(\frac{\partial h}{\partial x}\right)^2+\frac{2}{3}h\frac{\partial^2 h}{\partial x^2}\right]+\bar{\sigma}_x'(\rho gh\frac{h}{x})\left[\frac{1}{3}\left(\rho gh\frac{\partial h}{\partial x}\right)-\frac{4}{3}h\frac{\partial\bar{\sigma}_x'}{\partial x}\right]$$
$$-(\rho gh)^3\left(\frac{\partial h}{\partial x}\right)^2\left[\frac{3}{2}\left(\frac{\partial h}{\partial x}\right)^2+\frac{6}{5}h\frac{\partial^2 h}{\partial x^2}\right]-\frac{1}{\bar{A}}\frac{\partial u_b}{\partial x} \tag{13}$$

$$\frac{\partial(h\bar{u})}{\partial x}=\bar{A}h\left[\bar{\sigma}_x'^3+\rho gh\left(\frac{\partial h}{\partial x}\right)^2-\sigma^2+\frac{1}{3}\left(\rho gh\frac{\partial h}{\partial x}\right)^2\bar{\sigma}_x'+\frac{1}{2}(\rho gh)^3\left(\frac{\partial h}{\partial x}\right)^4\right]+u_b\frac{\partial h}{\partial x} \tag{12}$$

$$\frac{\partial(h\bar{u})}{\partial x}=\bar{b}-\bar{h} \tag{4}$$

plus a bottom-sliding relation describe nonsteady glacial flow.

EXISTENCE OF SOLUTION

The model equations (4), (12), and (13), plus a bottom-sliding relation, are highly nonlinear and difficult to solve analytically. It is not difficult, however, to show that these equations have a solution which uniquely specifies ice-sheet configuration for all positions, x, and times, t, if the initial configuration of the system and two boundary conditions are specified.

If $\bar{A}$ and ρ are known, then the flow-law equations (12) and (13) may be restated

$$\frac{\partial(h\bar{u})}{\partial x}=f_1(h,\frac{\partial h}{\partial x},\bar{\sigma}'_x,u_b) \tag{14}$$

$$0=f_2(\bar{\sigma}'_x,\frac{\partial\bar{\sigma}'_x}{\partial x},h,\frac{\partial h}{\partial x},\frac{\partial^2 h}{\partial x^2},\frac{\partial u_b}{\partial x}) \tag{15}$$

where f_i indicates some function of the variables listed. Dependence of (15) on the horizontal gradient in depth-averaged longitudinal-deviatoric stress is very weak and may be ignored.

Although bottom sliding is not well-understood, many published models agree in postulating that sliding velocity is a function of basal shear stress, which depends on ice thickness and surface slope, and of basal roughness (Weertman, 1957; 1964; Nye, 1969; 1970; Kamb, 1970; Lliboutry, 1975). If basal roughness can be calculated independently, from knowledge of bedrock characteristics and subglacial hydrology, then

$$u_b=f_3(h,\frac{\partial h}{\partial x}) \quad . \tag{16}$$

Substituting for $\bar{\sigma}'_x$ and u_b in (14) from (15) and (16) gives

$$\frac{\partial(h\bar{u})}{\partial x}=f_4(h,\frac{\partial h}{\partial x},\frac{\partial^2 h}{\partial x^2}) \quad . \tag{17}$$

If $\dot{b}$ is known, then equating (17) with the continuity equation (4), yields

$$\dot{h}=f_5(h,\frac{\partial h}{\partial x},\frac{\partial^2 h}{\partial x^2}) \quad . \tag{18}$$

Equation (18) has the solution

$$h=h(x,t) \tag{19}$$

which is uniquely determined if we specify the initial condition, h(x,0), and two boundary conditions. It has proven useful to specify the surface slope at the ice divide, $\frac{\partial h}{\partial x}(0,t)$, and thickness at the terminus, h(L,t), but other boundary conditions could be used.

EAST ANTARCTICA: STEADY STATE

As a first test, the model is applied to a flow line leading from Dome C to the coast in East Antarctica, which is assumed to be in steady-state with smoothed modern configuration. At least part of the base of the East Antarctic ice sheet is at the basal-melting temperature and free to slide (Oswald and Robin, 1973); however, ice velocity due to basal sliding is much less than velocity due to internal deformation (Appendix D), except in some places near the coast. Thus, it is assumed here that no bottom sliding occurs.

Ice-sheet configuration is approximated with the Vialov (1958) profile

$$h=H[1-(\frac{x}{L})^{4/3}]^{3/8} \tag{20}$$

which provides an excellent empirical fit. Here H=3500 m is thickness at the ice divide, and L=850 km is distance from the ice divide to the terminus. Accumulation-rate data from Bull (1971) may be approximated by

$$\dot{b}=5.4\times10^{-3}\exp(4.7\times10^{-6}x)+3.2\times10^{-2}\ \mathrm{ma}^{-1} \tag{21}$$

where x is in meters.

The modern ice sheet is assumed to be in steady state; that is, $\dot{h}=0$. The model equations (4), (12), and (13) are then solved, with bottom-sliding velocity equal to zero, for the horizontal gradient in horizontal ice flux, the depth-averaged longitudinal-deviatoric stress, and the depth-averaged flow-law parameter.

The flow-law parameter, $\bar{A}$, calculated in this manner is relatively constant at about $8 \times 10^{-25} (Nm^{-2})^{-3} s^{-1}$ in inland regions, and increases rapidly to $5 \times 10^{-24} (Nm^{-2})^{-3} s^{-1}$ near the coast. The calculated values of $\bar{A}$ correspond to temperatures of -8 to 0° C (Paterson, 1981, p. 39), which is reasonable considering that $\bar{A}$ is weighted to favor values near the bed where temperatures are high, and calculated values of $\bar{A}$ must be artifically high to allow for any bottom sliding that actually occurs. The increase in $\bar{A}$ toward the coast reflects both increasing temperature through the entire ice column and increasing importance of bottom sliding toward the coast.

Calculated values of depth-averaged longitudinal-deviatoric stress exhibit a broad minimum between about 100 km from the ice divide and 100 km from the terminus, with rapid increases at either end (Fig. 1). The increase in $\bar{\sigma}'_x$ toward the coast may be understood from a continuity argument: toward the coast total ice flux increases rapidly and thickness through which ice flows decreases rapidly, so that flow must become increasingly extensional even though $\bar{A}$ increases less-rapidly toward the coast.

Near the ice divide, shear stress tends to zero. For continuity of flow, where the shear stress is reduced there must be compensatingly larger values of longitudinal-deviatoric stress, so longitudinal-deviatoric stress increases toward the ice divide. It has been proposed that anisotropy in crystallographic orientation observed near ice divides (see, for example, Blankenship, 1982) where

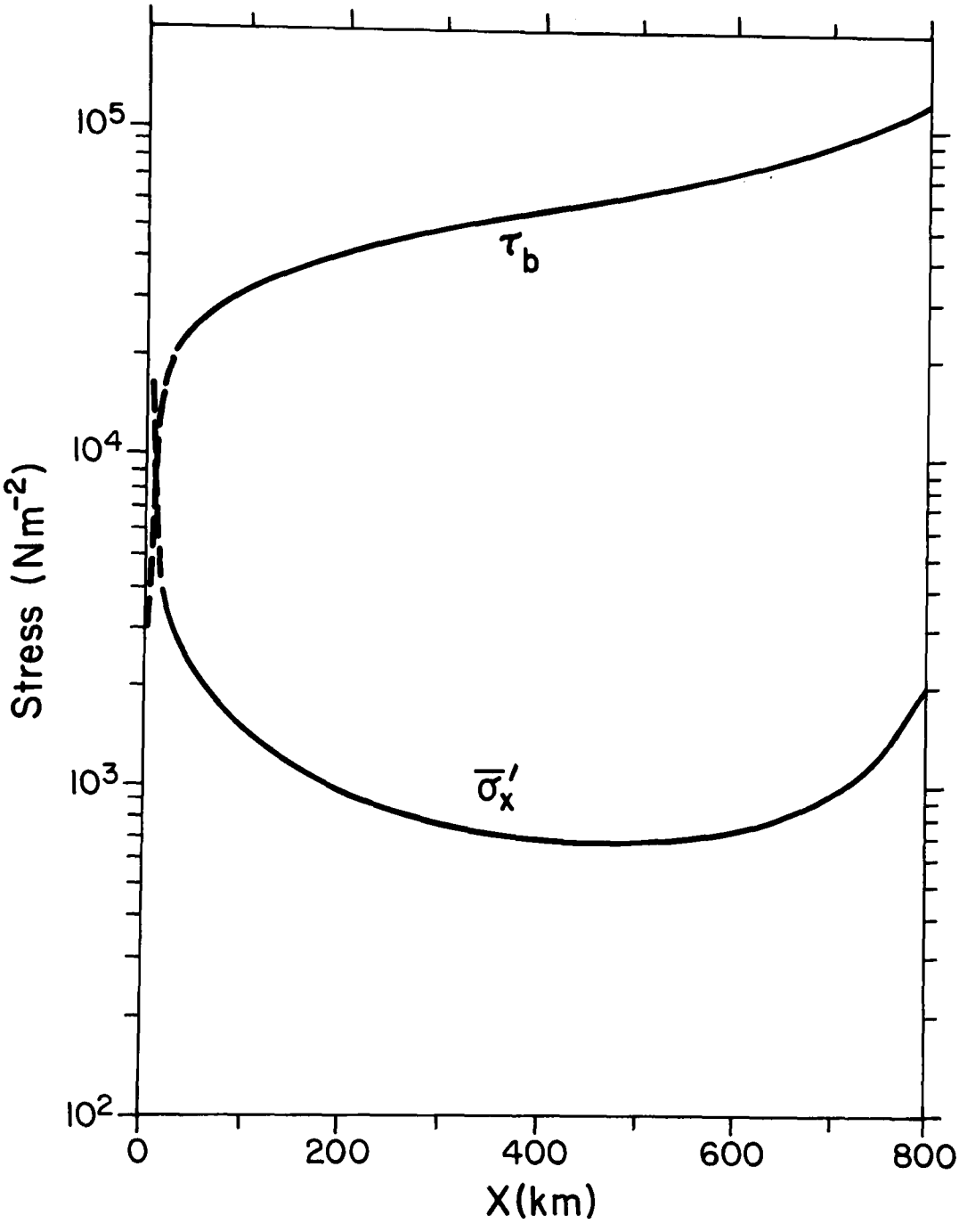

Figure 1. ,Calculated values of depth-averaged longitudinal-deviatoric stress ($\overline{\sigma}_x$) and basal shear stress (τ_b) along a flow line from Dome C to the coast, using modern smoothed configuration and accumulation-rate data, and assuming steady state.

shear stresses are small is caused by longitudinal extension (Hooke and Hudleston, 1980). The results here show that longitudinal stresses do increase rapidly near the ice divide, lending support to this hypothesis. Note that the increase in longitudinal stress toward the ice divide is also found in other models (Bolzan, 1984).

EAST ANARCTICA: NONSTEADY

Sea level was about 100 m lower during the Wisconsinan glacial maximum than today, which allowed the East Antarctic ice sheet to extend 75 to 90 km farther than its present limits onto the continental shelf (Hollin, 1962). Post-Wisconsinan sea-level rise between 15,000 years BP and 5,000 years BP (Milliman and Emery, 1968) caused the ice sheet to retreat to its present position. Grounding-line retreat caused a wave of thinning to propagate upglacier.

Mechanics of ice-sheet retreat caused by rising sea level have been modelled for marine ice sheets drained by ice streams (Thomas, 1977; Thomas and Bentley, 1978), but have not been modelled previously for a continental ice sheet. Near-coastal regions of the continental East Antarctic ice sheet are relatively warm with high accumulation rates, and fast-moving ice streams and outlet glaciers occur in some areas. Warm, high-accumulation regions with significant bottom sliding should respond rapidly to changes in sea level (Thomas and Bentley, 1978), causing a wave of adjustment to propagate upglacier.

To model this wave of adjustment along a typical flow line from Dome C to the coast, a Wisconsinan-maximum ice sheet is first generated with the Vialov (1958) profile extending to the edge of the continental shelf. Sea-level rise and grounding-line retreat are simulated by specifying the thickness at a point near the present coast, and causing it to thin over time. At the same time, changes in accumulation rate may be specified. The model calculates changes in

ice-sheet thickness, in response to thinning near the coast and changes in accumulation rate, as a function of position and time, assuming the position of the ice divide does not move.

Model results show that thinning near the coast causes a wave of adjustment to propagate upglacier with decreasing velocity, decreasing amplitude, and increasing diffusivity. To better understand this wave of adjustment, consider the Wisconsinan-maximum ice sheet with thickness at the ice divide H_w=3600 m, half-width L_w=930 km, and reduce thickness near the modern terminus to the modern value in 10 years beginning 15,000 years BP, while holding accumulation rate constant.

Results for constant accumulation rate are plotted in Figures 2 and 3. Total thinning is largest near the coast, and it decreases rapidly inland. The horizontal gradient in thinning becomes small near the ice divide. Upglacier diffusion and decrease in velocity and amplitude of the wave of adjustment are evident, especially in Figure 3.

Physically, a eustatic sea-level rise floats terminal regions of the ice sheet off the bed. This reduces total force opposing the flow upglacier of the new grounding line; since forces no longer balance, the glacier begins to flow faster and thins close to the grounding line. This acts in two ways: first, it increases longitudinal-deviatoric stress upglacier; and second, it increases surface slope and also shear stress at the upglacier end of the thinning ice. Both effects cause a wave of thinning to propagate upglacier. As the wave

Figure 2. Change in thickness (Δh) from Wisconsinan-maximum ice sheet, caused by sea-level rise in 10 years with no change in accumulation rate. Wisconsinan-maximum ice sheet has half-width L_w=930 km and thickness at the ice divide H_w=3600 m.

2a. Change in thickness from 10,000 to 15,000 years after onset of sea-level rise.

2b. Change in thickness from 5,000 to 10,000 years after onset of sea-level rise.

2c. Change in thickness from 1,000 to 5,000 years after onset of sea-level rise.

2d. Change in thickness from 100 to 1,000 years after onset of sea-level rise.

2e. Change in thickness from 0 to 100 years after onset of sea-level rise.

2f. Thickness (h) profiles for Wisconsinan-maximum ice sheet (labelled 0a) and for ice sheet after 15,000 years.

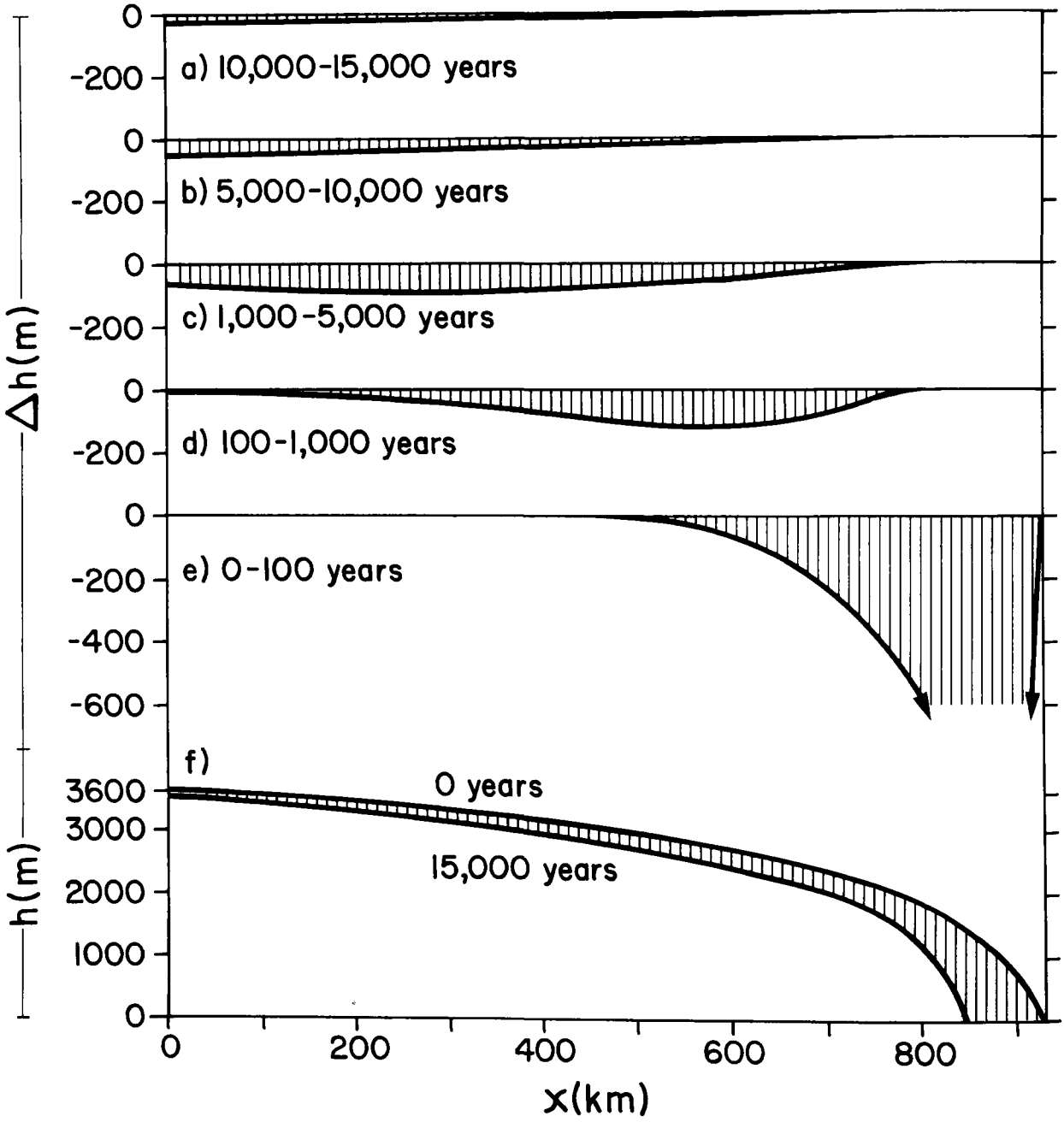
0
-200
a) 10,000-15,000 years
0
-200
b) 5,000-10,000 years
0
-200
c) 1,000-5,000 years
0
-200
d) 100-1,000 years
0
-200
-400
-600
e) 0-100 years
Δh(m)
f)
0 years
15,000 years
3600
3000
2000
1000
0
h(m)
0
200
400
600
800
x(km)

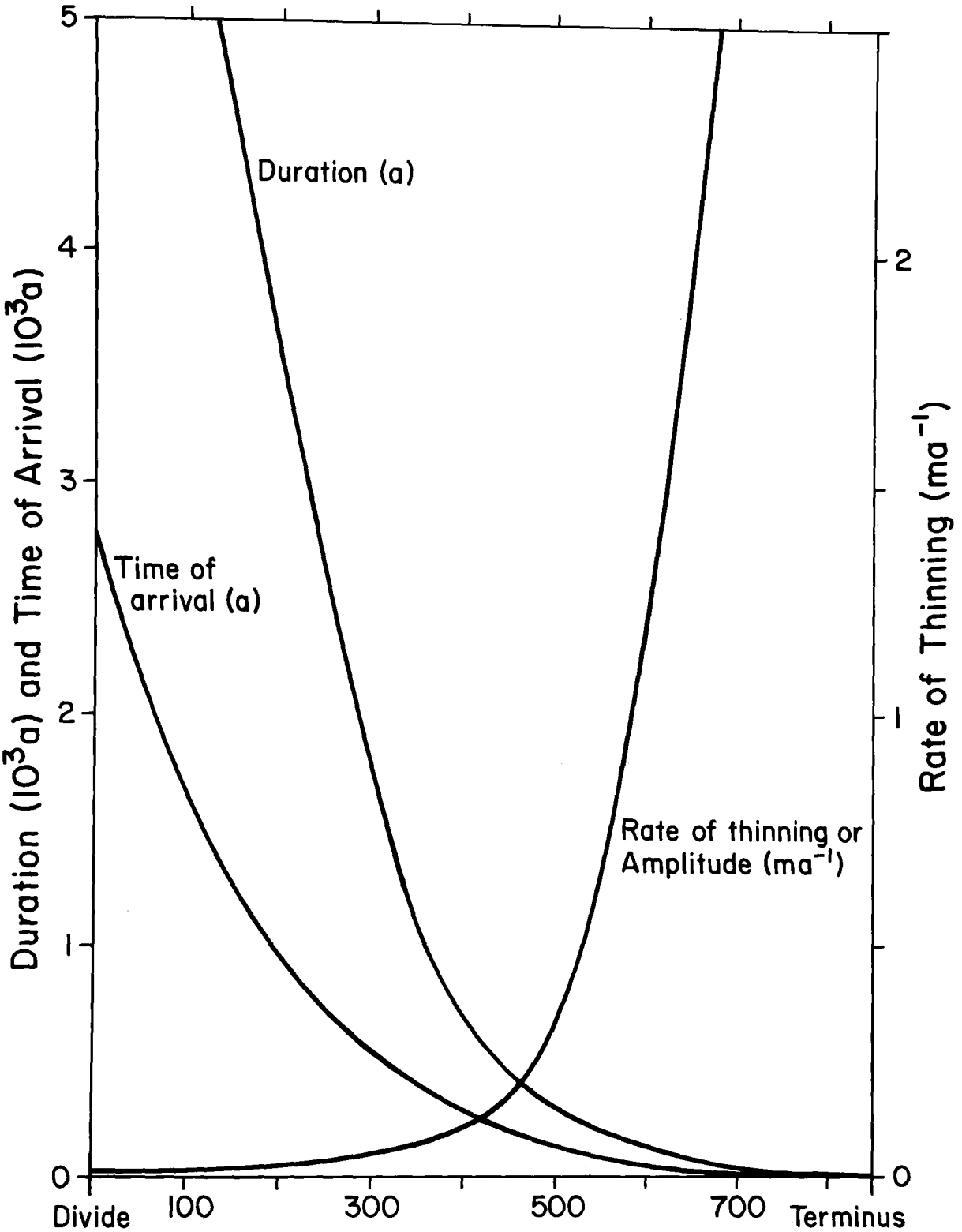

Figure 3. Characteristics of the wave of thinning shown in Figure 2. "Rate of thinning" or "amplitude" is the maximum rate of thinning that occurs at any point. "Duration" is the number of years at each position during which the rate of thinning is at least half of the maximum rate of thinning. "Time of arrival" is the number of years that elapse between onset of sea-level rise and the occurrence of the maximum rate of thinning at a position.

moves upglacier, the disturbance is spread over thicker, stiffer (smaller flow-law parameter, A) ice, so that the wave diffuses, damps, and slows down. Eventually, the ice sheet adjusts to a new profile in force equilibrium and mass balance, with reduced bed area.

In most regions of East Antarctica, flow is dominated by shear stress. A simplified version of the model presented here, in which longitudinal-deviatoric stress is taken to be identically zero everywhere, gives similar results to those obtained from the more-complete model. The wave of thinning caused by sea-level rise thus seems to propagate mainly by increased shear stress, with only a minor contribution from increased longitudinal-deviatoric stress. The dominant role of shear stress as compared to longitudinal-deviatoric stress is not surprising, because in deep layers of the ice sheet where most deformation occurs, longitudinal-deviatoric stresses are typically at least two orders of magnitude smaller than shear stresses, except near the ice divide (Fig. 1). Also, calculated values of $\bar{A}$ are adjusted to give initial steady-state in balance with stresses present. The simplified shear-stress-only model is quite similar to a two-dimensional version of the model of Mahaffy (1976). Thus, in regions where shear stress is dominant a Mahaffy-type model is accurate, although calculated values of $\bar{A}$ will not be as realistic as those from a model including longitudinal stresses. Where longitudinal stress is more important the more-complete model should give better results. The more-complete model provides better estimates of the depth-averaged flow-law parameter, $\bar{A}$.

Calculated total thinning near the ice divide 15,000 years after onset of sea-level rise (ΔH) depends on the thickness (H_w) and half-width (L_w) taken for the Wisconsinan-maximum ice sheet, the change in accumulation rate from the Wisconsinan to the Holocene ($\Delta \dot{b}$), and the time required for thinning at the terminal point (Δt_t). Among these parameters, $\Delta \dot{b}$ is most important.

Half-width of the Wisconsinan-maximum East Antarctic ice sheet is not well-constrained by geologic evidence. Several lines of geological and geophysical evidence indicate that the West Antarctic ice sheet advanced to the edge of the continental shelf during the Wisconsinan, and it is likely that the East Antarctic ice sheet exhibited similar behavior (Stuiver and others, 1981). Advance to the edge of the continental shelf would have amounted to 75 to 90 km in East Antarctica (Hollin, 1962). Values of ΔH corresponding to Wisconsinan advance of 75 km and of 90 km differ by only 20 m (Fig. 4).

Values of ΔH are sensitive both to time of onset of thinning at the coast and to duration of thinning. Onset of eustatic sea-level rise 15,000 years BP and duration of sea-level rise to 5,000 years BP are relatively well-constrained by the geologic record (Fairbridge, 1961; Shepard, 1963; Milliman and Emery, 1968; Mörner, 1971; Bloom and others, 1974). Near-coastal response to sea-level rise should be rapid (Thomas and Bentley, 1978) so that thinning should have occurred also between 15,000 and 5,000 years BP. Data on deglaciation in East Antarctica are scarce, but the ice had reached its present position by

Figure 4. Sensitivity of calculated thinning from Wisconsinan-maximum thickness at Dome C 15,000 years after onset of sea-level rise (ΔH) to variation of free parameters.

4a. Sensitivity to time required for sea-level rise (Δt_t), for Wisconsinan-maximum half-width L_w=930 km, and change in accumulation rate $\Delta \dot{b}$=0.

4b. Sensitivity to Wisconsinan-maximum half-width (L_w), for Δt_t=10,000 years and $\Delta \dot{b}$=0.

4c. Sensitivity to step increase in accumulation rate of $\Delta \dot{b}$ percent from Wisconsinan-maximum to modern value occurring 15,000 years BP, for Δt_t=10,000 years and L_w=930 km. Various estimates of $\Delta \dot{b}$ are:
1) approximately 10 percent increase calculated by J. Bolzan (1984);
2) little change in accumulation rate (Thompson and others, 1981);
3) 33 percent increase (Lorius and others, 1984);
4) 50 percent increase (Robin, 1977).

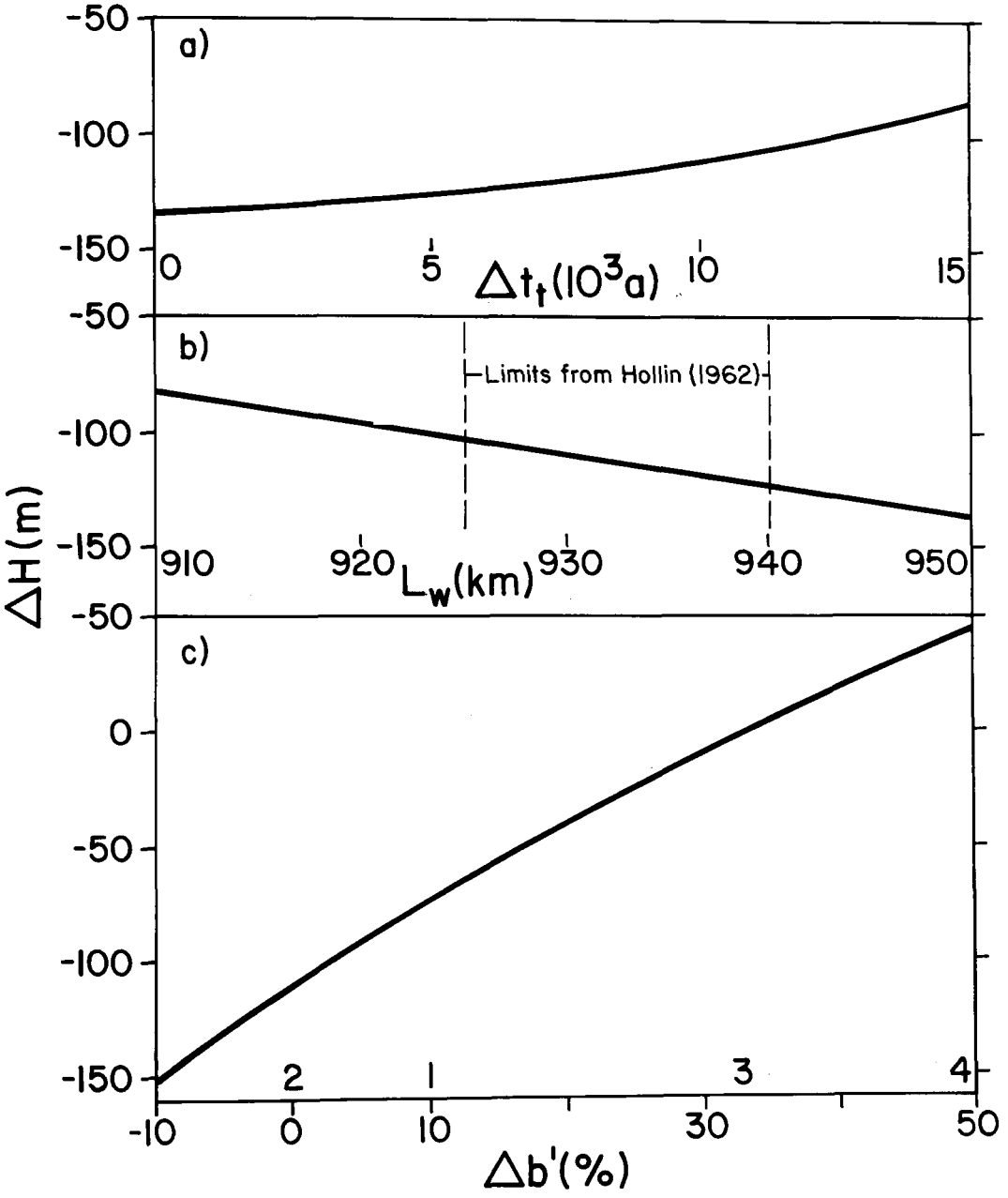
a)
b)
c)
-50
-100
-150
-50
-100
-150
-50
0
-50
-100
-150
0
5
10
15
$\Delta t_f(10^3 a)$
Limits from Hollin (1962)
910
920
930
940
950
L_w(km)
ΔH(m)
2
1
3
4
-10
0
10
30
50
Δb'(%)

about 6,000 years BP near Wilkes Station (Cameron and Goldthwait, 1961) and by about 3,800 years BP near the Ongul Islands (Meguro and others, 1963), thus being in reasonable agreement with the value assumed here of 5,000 years BP.

Values of ΔH are also sensitive to H_w; however, H_w is not a free parameter. For given values of $\Delta \dot{b}$, L_w, and Δt_t, H_w must be chosen to give the modern value of H after 15,000 years. Any one of the parameters $\Delta \dot{b}$, L_w, Δt_t, or H_w could be chosen to be dependent upon the other three; H_w is chosen as the dependent variable here because it is least constrained by data on the Wisconsinan-Holocene transition.

Accumulation rate may have changed from the Wisconsinan to the Holocene. Robin (1977) argues that an increase in temperature would have allowed greater transport of water vapor inland, causing a 50 percent to 100 percent increase in accumulation rate from Wisconsinan values. In contrast, annual-layer thicknesses at Dome C determined from microparticle concentrations show little change in accumulation rate from the Wisconsinan to the Holocene (Thompson and others, 1981). Lorius and others (1984) estimate a 33 percent increase in accumulation rate from Wisconsinan to Holocene. Combined interpretation of temperature and oxygen-isotopic data from Dome C and data from deep-sea sediment cores by Bolzan (1984) indicates approximately a 10 percent increase in accumulation rate from the Wisconsinan to the Holocene.

The model developed here allows calculation of change in thickness of the ice sheet due to the combined effects of sea-level rise and accumulation-rate change, for specified values of accumulation-rate

change. Results are shown in Figure 4. A step increase in accumulation rate 15,000 years BP has been assumed. The model ice sheet responds relatively rapidly to changes in accumulation rate, so the effect of a step change is very similar to the effect of a linear increase in accumulation rate from 15,000 years BP to 10,000 years BP. Model results show that sea-level rise combined with a 10 percent increase in accumulation rate gives 37 m less thinning than sea-level rise with no change in accumulation rate. This agrees well with results from other models that do not consider changes in sea level. A 10 percent increase in accumulation rate 15,000 years BP at Dome C gives thickening of about 41 m in the Nye (1960), Whillans (1981), and Bolzan (class II, n=2; 1984) models. Differences between these models are discussed in Appendix F.

If the accumulation rate at Dome C changed as suggested by Robin (1977), then the ice sheet has thickened there by more than 40 m since the Wisconsinan. If accumulation rates were higher during the Wisconsinan, then the ice sheet has thinned by more than 110 m. The most-likely change in accumulation rate is the 10 percent increase from Wisconsinan to Holocene suggested by Bolzan (1984), which gives a thinning of the ice sheet at Dome C of about 75 m over the last 15,000 years, due to the combined effects of both accumulation-rate and sea-level change.

For no change in accumulation rate, total thinning at Dome C due to sea-level rise has been about 110m over the last 15,000 years; about 40 m more thinning will occur during the next 15,000 years, with a total thinning of about 160 m at steady state.

The analysis here has assumed a much simpler physical system than that found in nature. In particular, nonplanar aspects of the bed, bottom sliding, temperature changes, secondary oscillations in sea-level rise, and isostatic rebound have been ignored.

All of these simplifications may be made without introducing significant errors because of the way the ice sheet responds to perturbations. Near-coastal regions respond rapidly, and inland regions respond slowly. Waves of adjustment are strongly slowed, damped, and diffused as they move inland, so only large, long-period events affect inland regions. Inland response is largely independent of the position of the perturbation if it occurs within 100 km of the coast.

Bottom sliding is important only near the coast, and the Wisconsinan-Holocene temperature changes already have affected ice-sheet flow near the coast (Whillans, 1981). Near-coastal response is almost instantaneous when compared to inland response, however, and any corrections introduced by allowing for bottom sliding and temperature changes near the coast would not significantly alter the results of the present calculations.

Delayed isostatic response may have allowed the grounding line to retreat farther inland and then readvance to its present position as the bed rose isostatically. The magnitude of this effect is difficult to assess; however, it is likely that it would have been smaller than

the first-order effect modelled here. Furthermore there were also short-period oscillations of sea level (Fairbridge, 1961; Mörner, 1971), and these probably caused small near-coastal oscillations in the ice sheet. Such small oscillations in the ice sheet near the coast are damped and diffused as they move upglacier, and have little effect on inland response.

Slow inland response applies to temperature changes as well as to waves of adjustment travelling upglacier. Post-Wisconsinan warming has not penetrated sufficiently far into the ice sheet in inland regions to affect flow and cause ice-sheet thinning (Whillans, 1981).

The bed of the East Antarctic ice sheet is not, in general, horizontal (Drewry, 1982). The bed is reasonably horizontal, however, when averaged on a grid spacing of about 40 km, such as is used here.

Thus, the rapid near-coastal response and slow inland response of the ice sheet, and the strong damping and diffusion of waves of adjustment moving upglacier, allow inland response to be modelled as a simple system, if bed elevation is averaged over a wide grid-point spacing.

Data or independent model results are scarce to test the conclusion that 75 m of total thinning has occurred at Dome C over the last 15,000 years, but in general support this conclusion. Model results of Hughes and others (1981) show the Wisconsinan-maximum East Antarctic ice sheet to be 100 to 200 m thicker than the modern in the vicinity of Dome C; however, they consider this to be a maximum

thickness because it does not allow for smaller accumulation rates during the Wisconsinan, and because it assumes that the modern and Wisconsinan-maximum ice sheets represent equilibrium configurations. For no change in accumulation rate, the model developed here gives total post-Wisconsinan thinning to a steady configuration of 160 m, in good agreement with the results of Hughes and others (1981). The model results here also support the supposition of Hughes and others (1981) that changes in accumulation rate and nonsteady effects are important.

Data on Wisconsinan-maximum thickness of the inland East Antarctic ice sheet are limited to glacial-geological results on outlet glaciers through the Transantarctic Mountains. Morainal deposits at the heads of the Reedy and Beardmore glaciers show that the East Antarctic ice sheet was only 30 to 40 m thicker during the Wisconsinan than today (Mercer, 1968; 1972). These results are not immediately interpretable in terms of thickness changes at Dome C, because the Reedy and Beardmore glaciers do not lie on flow lines from Dome C. The results are consistent with modest thinning of the East Antarctic ice sheet since the Wisconsinan, as is indicated by model results presented here.

The most direct way to test the results obtained here would be to obtain dated, unfractured core samples from Dome C and regions downglacier, measure total gas content, and calculate how thickness

has changed (Raynaud, 1976). Detailed studies of sediments and gravity anomalies on the continental shelf adjacent to East Antarctica, and further glacial-geological studies of outlet glaciers through the Transantarctic Mountains, might provide information on the former extent and thickness of the East Antarctic ice sheet.

CONCLUSIONS

For a continental ice sheet with grounding-line position or outer limit controlled by sea level, a rise in sea level causes a wave of thinning to propagate upglacier. The velocity and amplitude of the wave decrease upglacier, and it diffuses rapidly. Thus, perturbations near the coast must be large and have long periods to have important effects on inland regions of the ice sheet, and inland response is similar regardless of the details of perturbations if they occur within 100 km of the coast.

Thinning at Dome C, East Antarctica, due to post-Wisconsinan sea-level rise has been about 110 m, and is now largely completed. For each 10 percent that accumulation increased from Wisconsinan to Holocene, total post-Wisconsinan thinning is reduced by about 35 m. The most-likely scenario is a 10 percent increase in accumulation rate, and about 75 m of total post-Wisconsinan thinning is due to the combined effects of sealevel rise and accumulation-rate change.

Thin, high-accumulation, warm ice sheets with significant basal sliding should respond more rapidly to changes in sea level and accumulation rate than thick, low-accumulation, cold ice sheets frozen to their beds. Thus, the West Antarctic ice sheet and the former Laurentide ice sheet would respond more rapidly than the East Antarctic ice sheet.

The model developed here provides a simple way to consider longitudinal-deviatoric stress in ice flow. If the bottom-sliding relation is specified as a function of position, then the model is equally valid for an ice stream, an ice sheet sliding over its bed, or an ice sheet frozen to its bed. The entirety of a flow line passing from an ice divide through shear-dominated regions with or without basal sliding and then an ice stream to the grounding line can be treated with this model.

LIST OF APPENDICES

Appendix A. Demonstration that $\frac{\partial u}{\partial z} >> \frac{\partial w}{\partial x}$.

The shear-flow law for flow in the x-z plane with exponent equal to three is written properly as (Paterson, 1981, p. 84-85)

$$\dot{\varepsilon}_{xz} = A \tau_e^{\,2} \tau_{xz} \tag{A1}$$

where the effective stress, τ_e, is given by

$$\tau_e^{\,2} = \tau_{xz}^{\,2} + \sigma_x'^{\,2} \tag{A2}$$

and the shear-strain rate, $\dot{\varepsilon}_{xz}$, is given by

$$\dot{\varepsilon}_{xz} = \frac{1}{2}\left(\frac{\partial u}{\partial z} + \frac{\partial w}{\partial x}\right) \tag{A3}$$

with u and w representing the horizontal component of velocity and the magnitude of the vertical component of velocity, respectively.

Combining (A1)-(A3) gives

$$\frac{\partial u}{\partial z} + \frac{\partial w}{\partial x} = 2A\left(\tau_{xz}^{\,3} + \sigma_x'^{\,2} \tau_{xz}\right) \quad . \tag{A4}$$

In developing the model, this was taken to be

$$\frac{\partial u}{\partial z} = 2A\left(\tau_{xz}^{\,3} + \sigma_x'^{\,2} \tau_{xz}\right) \quad ; \tag{A5}$$

that is, it was assumed that

$$\frac{\partial u}{\partial z} >> \frac{\partial w}{\partial x} \quad . \tag{A6}$$

This assumption is justified below for the shear-dominated East Antarctic ice sheet and for an ice stream. The general approach is to use simplified ice-flow models to estimate maximum values of the

horizontal gradient in vertical velocity, $(\frac{\partial w}{\partial x})_m$, and typical values of the vertical gradient in horizontal velocity, $(\frac{\partial u}{\partial z})_t$, and to demonstrate that

$$(\frac{\partial u}{\partial z})_t >> (\frac{\partial w}{\partial x})_m \qquad \text{(A7)}$$

If (A7) is true, then (A6) must also be true for most of the ice sheet.

Ai. East Antarctica downglacier from Dome C.

Assume two-dimensional flow over a horizontal bed, with bottom melting much less than surface accumulation. Then vertical velocity is equal to zero at the bed, increasing to a maximum value $w=w_m$ at the surface. Vertical velocity at the surface is due both to accumulation rate and to flow down the surface slope, so that

$$w_m=\dot{b}-u_s\frac{\partial h}{\partial x} \tag{A8}$$

where u_s is the value of u at the surface.

Differentiating (A8) with respect to x yields

$$\frac{\partial w_m}{\partial x}=\frac{\partial \dot{b}}{\partial x}-u_s\frac{\partial^2 h}{\partial x^2}-\frac{\partial u_s}{\partial x}\frac{\partial h}{\partial x} \quad . \tag{A9}$$

For $w=w_m$ at the surface, decreasing smoothly to w=0 at the bed, it is reasonable that

$$\frac{\partial w_m}{\partial x}=\left(\frac{\partial w}{\partial x}\right)_m \quad . \tag{A10}$$

The terms $\frac{\partial \dot{b}}{\partial x}$, $\frac{\partial h}{\partial x}$, and $\frac{\partial^2 h}{\partial x^2}$, in (A9) can be evaluated from measured accumulation rate and ice-sheet profile. It remains to calculate u_s and $\frac{\partial u_s}{\partial x}$ to allow evaluation of $\left(\frac{\partial w}{\partial x}\right)_m$.

Horizontal velocity varies with depth rapidly near the bed and slowly near the surface (Nye, 1959) so that

$$u_s > 2\bar{u} \tag{A11}$$

where $\bar{u}$ is the horizontal velocity averaged over ice thickness. In a steady-state ice sheet, $\bar{u}$ can be calculated from the continuity equation

$$\bar{u} = \frac{1}{h}\int_o^x b\,dx' \quad . \tag{A12}$$

Combining (A9)-(A11) yields

$$\left(\frac{\partial w}{\partial x}\right)_m = \frac{\partial b}{\partial x} - 2\bar{u}\frac{\partial^2 h}{\partial x^2} - 2\frac{\partial \bar{u}}{\partial x}\frac{\partial h}{\partial x} \tag{A13}$$

where $\bar{u}$ and its derivative with respect to x are calculated from (A12).

Next, a typical value of the vertical gradient in horizontal velocity, $\left(\frac{\partial u}{\partial z}\right)_t$, is calculated. It is assumed that u varies linearly with depth from u=0 at the bed to u=2$\bar{u}$ at the surface; this underestimates $\frac{\partial u}{\partial z}$ in deep layers where most deformation occurs, and overestimates $\frac{u}{z}$ near the surface. Then

$$\left(\frac{\partial u}{\partial z}\right)_t = \frac{2\bar{u}}{h} \tag{A14}$$

or, substituting from (A12)

$$\left(\frac{\partial u}{\partial z}\right)_t = \frac{2}{h^2}\int_o^x b\,dx' \quad . \tag{A15}$$

The ice-sheet configuration from Dome C to the coast may be approximated by the Vialov (1958) profile

$$h=H[1-(\frac{x}{L})^{4/3}]^{3/8} \tag{A16}$$

and first and second derivatives with respect to x are taken from this. Here L=850 km is the modern half-width and H=3500 m is the modern thickness at the ice divide. Accumulation-rate date from Bull (1971) may be approximated by

$$\dot{b}=1.76\text{x}10^{-10}\exp(4.70\text{x}10^{-6}\text{x})+1.00\text{x}10^{-9}\ \text{ms}^{-1} \tag{A17}$$

and the first derivative with respect to x is obtained from this. From (A12), (A16), and (A17)

$$\bar{u}=\frac{1}{H}[1-(\frac{x}{L})^{4/3}]^{-3/8}\{3.74\text{x}10^{-5}[\exp(4.70\text{x}10^{-6}\text{x})-1] +1.00\text{x}10^{-9}\text{x}\ \text{ms}^{-1} \tag{A18}$$

whence

$$\frac{\partial\bar{u}}{\partial x}=\frac{1}{H}[1-(\frac{x}{L})^{4/3}]^{-3/8}[1.76\text{x}10^{-10}\exp(4.70\text{x}10^{-6}\text{x})+1.00\text{x}10^{-9}] +\frac{x^{1/3}}{2HL^{4/3}}[1-(\frac{x}{L})^{4/3}]^{-3/8}\{3.74\text{x}10^{-5}[\exp(4.70\text{x}10^{-6}\text{x})-1] +1.00\text{x}10^{-9}\text{x}\}\text{s}^{-1} \tag{A19}$$

It is now possible to evaluate $(\frac{\partial w}{\partial x})_m$ and $(\frac{\partial u}{\partial z})_t$ according to (A13) and (A15), using (A16)-(A19). These calculations are shown in table AI for three points along a flow line from Dome C to the coast. It is

Table AI. Calculation of $(\frac{\partial w}{\partial x})_m$ and $(\frac{\partial u}{\partial z})_t$ for East Antarctica.

Parameter	Equation	Values		
$x(m)$		$0.10\times10^{+5}$	$4.25\times10^{+5}$	$8.40\times10^{+5}$
$\bar{u}(ms^{-1})$	(A18)	3.37×10^{-9}	2.29×10^{-7}	3.72×10^{-6}
$\frac{\partial \bar{u}}{\partial x}(s^{-1})$	(A19)	3.39×10^{-13}	9.00×10^{-13}	1.59×10^{-11}
$\bar{b}(ms^{-1})$	(A17)	1.18×10^{-9}	2.30×10^{-9}	1.01×10^{-8}
$\frac{\partial \bar{b}}{\partial x}(s^{-1})$	(A17)	8.66×10^{-16}	6.09×10^{-15}	4.29×10^{-14}
$h(m)$	(A16)	$3.50\times10^{+3}$	$2.90\times10^{+3}$	$7.40\times10^{+2}$
$\frac{\partial h}{\partial x}$	(A16)	-4.69×10^{-4}	-2.24×10^{-3}	-2.76×10^{-2}
$\frac{\partial^2 h}{\partial x^2}(m^{-1})$	(A16)	-1.57×10^{-8}	-4.65×10^{-9}	-1.73×10^{-6}
$(\frac{\partial u}{\partial z})_t(s^{-1})$	(A15)	1.93×10^{-12}	1.58×10^{-10}	1.01×10^{-8}
$(\frac{\partial w}{\partial x})_m(s^{-1})$	(A13)	1.29×10^{-15}	1.23×10^{-14}	1.38×10^{-11}
$(\frac{\partial w}{\partial x})_m/(\frac{\partial u}{\partial z})_t$		6.68×10^{-4}	7.78×10^{-5}	1.37×10^{-3}

apparent that maximum values of $\frac{\partial w}{\partial x}$ are less than 0.2 percent of typical values of $\frac{\partial u}{\partial z}$ along the flow line, so that

$$\frac{\partial u}{\partial z} >> \frac{\partial w}{\partial x} \tag{A6}$$

is valid for East Antarctica.

Aii. West Antarctic ice streams.

Ice streams draining into the Ross Ice Shelf from the West Antarctic ice sheet flow through shallow, smooth bedrock troughs, and are recognizable for 300 km or more upglacier of the grounding line. When smoothed on a scale of 50 km, ice-stream beds are horizontal and surface slopes are constant (Jankowski and Drewry, 1981).

The origin is taken to be on the bed 300 km upglacier of the grounding line, x axis horizontal along a flow line, and z axis vertical. Then, to good approximation,

$$h=1360-.002x \tag{A20}$$

so that surface slope is constant and the second derivative of thickness with respect to x is zero.

Accumulation-rate data are scarce, but interpolating from Bull (1971) yields

$$\dot{b}=4.75\times10^{-9}\,ms^{-1}$$
$$\dot{b}=0.15\,ma^{-1} \tag{A21}$$

Basal-melting rate is on the order of $0.02\,ma^{-1}$ or less (Weertman and Birchfield, 1981) which is within probable errors in accumulation-rate estimates. Basal melting may increase slowly downglacier, but Bull (1971) shows accumulation rate increasing slowly downglacier, so net accumulation rate is about constant.

Equations (A9) and (A10) relating $(\frac{\partial w}{\partial x})_m$ and $(\frac{\partial u}{\partial z})_t$ are equally valid for ice streams as for shear-dominated ice sheets. Using (A20)

and (A21) these become

$$(\frac{\partial w}{\partial x})_m = 4x10^{-3}\frac{\partial \bar{u}}{\partial x} \quad . \tag{A22}$$

A balance calculation for West Antarctica shows to good approximation

$$\bar{u}_o = 6.3x10^{-6} ms^{-1}$$

$$\bar{u}_o = 200 ma^{-1} \tag{A23}$$

where the subscript $(_o)$ indicates the value at x=0. Steady-state continuity requires that

$$\bar{u} = \frac{1}{h}(\dot{b}x + h_o \bar{u}_o) \quad . \tag{A24}$$

Then

$$\frac{\partial \bar{u}}{\partial x} = \frac{1}{h^2}(h\dot{b} - \dot{b}\frac{\partial h}{\partial x}x - h_o \bar{u}_o \frac{\partial h}{\partial x}) \quad . \tag{A25}$$

Equation (A25) allows evaluation of $(\frac{\partial w}{\partial x})_m$ from (A22).

Next, it is necessary to calculate $\frac{\partial u}{\partial z}$. The shear-flow law may be written

$$\frac{\partial u}{\partial x} + \frac{\partial w}{\partial z} = \bar{A}\rho g \frac{\partial h}{\partial x}[\bar{\sigma}_x'^2(h-z) + (\rho g \frac{\partial h}{\partial x})^2(h-z)^3] \tag{A26}$$

where the assumptions $\sigma_x' = \bar{\sigma}_x'$ and $A = \bar{A}$ have been made (Appendices B and C). Integrating (A26) through thickness yields

$$\overline{(\frac{\partial u}{\partial z})} + \overline{(\frac{\partial w}{\partial x})} = 2\bar{A}\rho g \frac{\partial h}{x}[\bar{\sigma}_x'^2(h-z) + (\rho g \frac{\partial h}{\partial x})^2(h-z)^3] \tag{A27}$$

where the bar signifies an average over depth. Replacing $\overline{(\frac{\partial w}{\partial x})}$ by $(\frac{\partial w}{\partial x})_m$ in (A33) will underestimate $\overline{(\frac{\partial u}{\partial z})}$, and so strengthen the eventual conclusions.

It remains to calculate $\bar{\sigma}'_x$. In East Antarctica, $\bar{\sigma}'_x$ is on the order of $10^3 Nm^{-2}$. In an unconfined ice shelf, the balance of stresses with sea water gives $\bar{\sigma}'_x$ up to $10^6 Nm^{-2}$. A value between 10^3 and $10^6 Nm^{-2}$ is probably reasonable for ice streams.

Suppose that all ice motion is due to sliding over the bed ($u=u_b$; Weertman and Birchfield, 1981; Appendix C). Then the flow law yields

$$u=\bar{u} \tag{A28}$$

and

$$\frac{\partial u}{\partial x}=\bar{A}\bar{\sigma}'^3_x \tag{A29}$$

A good estimate of the flow-law parameter, $\bar{A}$, is $5\times10^{-25}(Nm^{-2})^{-3}s^{-1}$. This is the value determined by Thomas (1973) for ice-shelf spreading and is the value recommended by Paterson (1981, p.39) for -10 ^oC. Using this value of $\bar{A}$ and calculated values of $(\frac{\partial w}{\partial x})_m$, (A25), (A27), and (A28) can be solved for $\overline{(\frac{\partial u}{\partial z})}=(\frac{\partial u}{\partial z})_t$. Results are shown in table AII.

Table AII. Calculation of $(\frac{\partial w}{\partial x})_m$ and $(\frac{\partial u}{\partial z})_t$ for West Antarctic ice streams.

Parameter	Equation	Values		
x(m)		$0.0\times10^{+0}$	$1.5\times10^{+5}$	$3.00\times10^{+5}$
$\frac{\partial u}{\partial x}(s^{-1})$	(A25)	1.28×10^{-11}	2.10×10^{-11}	4.09×10^{-11}
$\bar{\sigma}'_x(Nm^{-2})$	(A28)	$2.95\times10^{+4}$	$3.48\times10^{+4}$	$4.34\times10^{+4}$
h(m)	(A20)	$1.36\times10^{+3}$	$1.06\times10^{+3}$	$7.60\times10^{+2}$
$\frac{\partial h}{\partial x}$	(A20)	-2.00×10^{-3}	-2.00×10^{-3}	-2.00×10^{-3}
$\dot{b}(ms^{-1})$	(A21)	4.75×10^{-9}	4.75×10^{-9}	4.75×10^{-9}
$(\frac{\partial w}{\partial x})_m(s^{-1})$	(A22)	5.12×10^{-14}	8.40×10^{-14}	1.64×10^{-13}
$(\frac{\partial u}{\partial z})_t(s^{-1})$	(A27)	1.76×10^{-11}	1.47×10^{-11}	1.38×10^{-11}
$(\frac{\partial w}{\partial x})_m/(\frac{\partial u}{\partial z})_t$		2.91×10^{-3}	5.71×10^{-3}	1.19×10^{-2}

From table AII it is evident that $(\frac{\partial w}{\partial x})_m$ is less than 1.2 percent of $(\frac{\partial u}{\partial z})_t$ in ice streams. Thus, it is valid to assume that

$$\frac{u}{z} \quad \frac{w}{x} \tag{A1}$$

for ice streams as well as for East Antarctica. It is probably valid to make this assumption for all grounded ice in polar ice sheets.

Appendix B. Similarity of different weighting schemes for flow-law parameter $\bar{A}$.

In the derivation of the model, it was assumed that $A=\bar{A}$, and the flow-law parameter was not explicitly averaged over depth as were other terms in the flow-law equations for shearing and longitudinal deformation. If A had been explicitly averaged over depth, different weighting by the shear and longitudinal flow laws would have led to different values of $\bar{A}$. In both cases $\bar{A}$ is weighted toward deeper layers, however, and the following discussion shows that different values of $\bar{A}$ differ by only a small amount.

Suppose that

$$A=A_o[1-(\frac{z}{h})^m] \tag{B1}$$

that is, A has a maximum value of A_o at the bed and decreases to zero at the surface. This model provides a reasonable fit to expected values, and makes calculations easy. For East Antarctica along a flow line from Dome C to the coast, H=3000 m and m=0.05 are reasonable values; m=0.01 is too small, but m=0.1 might be possible (Fig. B1).

From the flow law

$$\frac{\partial u}{\partial z}=2A\tau_e^{\,2}\tau_{xz} \tag{B2}$$

$$\frac{\partial u}{\partial x}=A\tau_e^{\,2}\sigma'_x \tag{B3}$$

where

$$\tau_e^{\,2}=\tau_{xz}^{\,2}+\sigma'^{\,2}_x \quad . \tag{B4}$$

Figure B1. Estimates of flow-law parameter, A, as a function of depth 425 km downglacier from Dome C. "Best values" are obtained using a Robin (1955) temperature model and the temperature-dependence of A recommended by Paterson (1981, p.39). Other curves are fits to the best values using the formula (B1), for different values of the constant m.

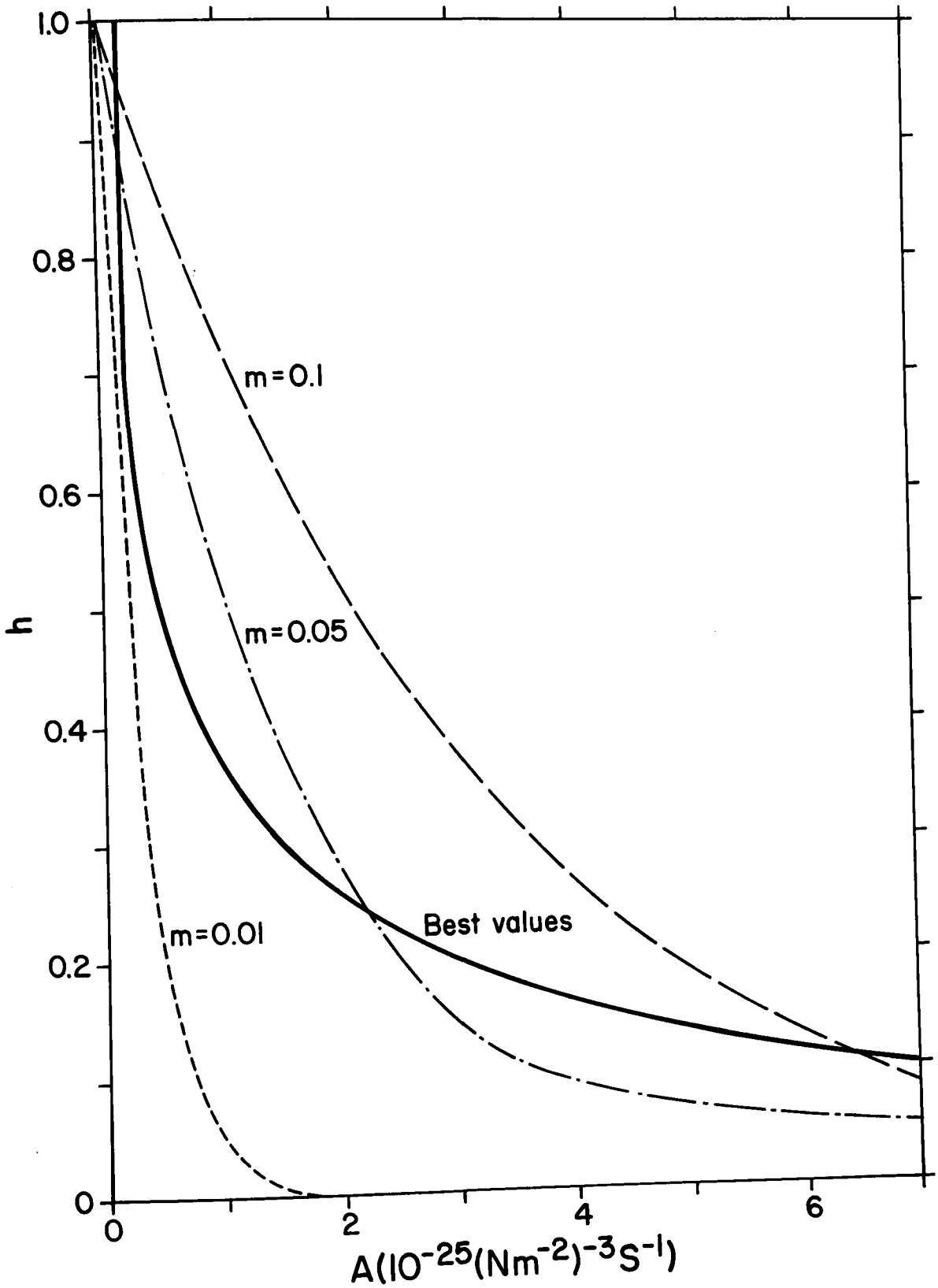
1.0
0.8
0.6
0.4
0.2
0
h
m=0.1
m=0.05
m=0.01
Best values
0
2
4
6
A(10^-25(Nm^-2)^-3S^-1)

First consider the case where $\sigma_x'=0$. The shear flow law (B2) gives

$$u=2\int_o^h A_o[1-(\frac{z}{h})^m](\rho g\frac{\partial h}{\partial x})^3(h^3-3h^2z+3hz^2-z^3)dz+u_b \tag{B5}$$

whence

$$u=2A_o(\rho g\frac{\partial h}{\partial x})^3[(h^3z-\frac{3}{2}h^2z^2+hz^3-\frac{z^4}{4})-\frac{1}{h^m}(\frac{h^3z^{m+1}}{m+1}-\frac{3h^2z^{m+2}}{m+2}+\frac{3hz^{m+3}}{m+3}-\frac{z^{m+4}}{m+4})]$$
$$+u_b \quad . \tag{B6}$$

Integrating (B6) through thickness gives

$$\bar{u}h=\frac{2}{5}A_o(\rho g\frac{\partial h}{\partial x})^3h^5[1-\frac{120}{(m+1)(m+2)(m+3)(m+4)(m+5)}]+u_bh \quad . \tag{B7}$$

Had it been assumed that $A=\bar{A}_1$ in (B2), then (B7) would have been

$$\bar{u}h=\frac{2}{5}\bar{A}_1(\rho g\frac{\partial h}{\partial x})^3h^5+u_bh \tag{B8}$$

so that

$$\bar{A}_1=A_o[1-\frac{120}{(m+1)(m+2)(m+3)(m+4)(m+5)}] \quad . \tag{B9}$$

Integrating the longitudinal flow law (B3) through thickness and then taking $\sigma_x'=0$ gives

$$\frac{\partial(h\bar{u})}{\partial x}=u(h)\frac{\partial h}{\partial x} \quad . \tag{B10}$$

Evaluating the horizontal velocity at the surface from (B6) and combining with (B10) yields

$$\frac{\partial(h\bar{u})}{\partial x}=\frac{1}{2}A_o(\rho g)^3(h\frac{\partial h}{\partial x})^4[1-\frac{24}{(m+1)(m+2)(m+3)(m+4)}]+u_b\frac{\partial h}{\partial x} \quad . \tag{B11}$$

Had it been assumed that $A=\bar{A}_2$ in (B2), then (B11) would have been

$$\frac{\partial(h\bar{u})}{\partial x}=\frac{1}{2}\bar{A}_2(\rho g)^3\left(h\frac{\partial h}{\partial x}\right)^4+u_b\frac{\partial h}{\partial x} \tag{B12}$$

so that

$$\bar{A}_2=A_o\left[1-\frac{24}{(m+1)(m+2)(m+3)(m+4)}\right] \quad . \tag{B13}$$

Both $\bar{A}_1$ and $\bar{A}_2$ are weighted according to the shear flow law for $\sigma_x'=0$; however, $\bar{A}_1$ requires integration over depth and then thickness, whereas $\bar{A}_2$ requires integration over thickness only. For m between 0.01 and 0.10, the difference between $\bar{A}_1$ and $\bar{A}_2$ ranges from 9 percent to 8 percent. Errors in determination of A_o are probably much larger than this (Paterson, 1981, p.34-40), so differences in the two weighting schemes are not significant.

Now consider $\sigma_x'=\bar{\sigma}_x'\neq 0$. This is more realistic, but leads to greater complications and a less-straightforward result.

First, the horizontal gradient in horizontal ice flux is derived from the shear-flow law (B2) by substituting (B4) and (B1) into (B2), integrating over depth and then over thickness, and differentiating with respect to x, assuming that horizontal variation of A is slow.

This gives

$$\frac{\partial(h\bar{u})}{\partial x} =$$

$$A_o\{[1-\frac{6}{(m+1)(m+2)(m+3)}][\bar{\sigma}_x'^2(\frac{2}{3}\rho g h^3\frac{\partial^2 h}{\partial x^2}+2\rho g(h\frac{\partial h}{\partial x})^2)+\bar{\sigma}_x'(\frac{4}{3}\rho g h^3\frac{\partial h}{\partial x}\frac{\bar{\sigma}_x'}{\partial x})]$$

$$+[1-\frac{120}{(m+1)(m+2)(m+3)(m+4)(m+5)}][(\rho g)^3 h^4(\frac{\partial h}{\partial x})^2(2(\frac{\partial h}{\partial x})^2+\frac{6}{5}h\frac{\partial^2 h}{\partial x^2})]\}$$

$$+\frac{\partial(hu_b)}{\partial x} \qquad \text{(B14)}$$

Had it been assumed that $A=\bar{A}_1$ in (B2), (B14) would have been

$$\frac{\partial(h\bar{u})}{\partial x}=\bar{A}_1\{\bar{\sigma}_x'^2[\frac{2}{3}\rho g h^3\frac{\partial^2 h}{\partial x^2}+2\rho g(h\frac{\partial h}{\partial x})^2]+\bar{\sigma}_x'[\frac{4}{3}\rho g h^3\frac{\partial h}{\partial x}\frac{\bar{\sigma}_x}{\partial x}]$$

$$+[(\rho g)^3 h^4(\frac{\partial h}{\partial x})^2][2(\frac{\partial h}{\partial x})^2+\frac{6}{5}h\frac{\partial^2 h}{\partial x^2}]\}+\frac{\partial(hu_b)}{\partial x} \qquad \text{(B15)}$$

There no longer exists a simple expression for $\bar{A}_1$ in terms of the constants A_o and m. Reasonable values of parameters for East Antarctica are:

$$h=3000m;\ \frac{\partial h}{\partial x}=-2\times10^{-3};\ \frac{\partial^2 h}{\partial x^2}=-4\times10^{-8};\ u_b=0;\ \bar{\sigma}_x'=700Nm^{-2};\ \frac{\partial\bar{\sigma}_x'}{\partial x}=0.$$

Substituting these values into (B14) and (B15) and eliminating insignificant terms yields

$$\frac{\partial(h\bar{u})}{\partial x}\sim A_o[1-\frac{120}{(m+1)(m+2)(m+3)(m+4)}]\frac{6}{5}(\rho g)^3 h^5(\frac{\partial h}{\partial x})^2(\frac{\partial^2 h}{\partial x^2}) \qquad \text{(B16)}$$

$$\frac{\partial(h\bar{u})}{\partial x}\sim\bar{A}_1\frac{6}{5}(\rho g)^3 h^5(\frac{\partial h}{\partial x})^2(\frac{\partial^2 h}{\partial x^2}) \qquad \text{(B17)}$$

so that

$$\bar{A}_1 \sim A_o\left[1-\frac{120}{(m+1)(m+2)(m+3)(m+4)}\right] \quad . \tag{B18}$$

Next, the horizontal gradient in horizontal ice flux is derived from the longitudinal flow law (B3) by substituting (B4) and (B1) into (B3), integrating through thickness, and evaluating u(h) from the shear flow law. This gives

$$\begin{aligned}\frac{\partial(h\bar{u})}{\partial x}=A_o\Big\{&\bar{\sigma}_x'^3 h\left[1-\frac{1}{m+1}\right]+\bar{\sigma}_x'^2\rho g\left(h\frac{\partial h}{\partial x}\right)^2\left[1-\frac{2}{(m+1)(m+2)}\right]\\ &+\bar{\sigma}_x'\frac{1}{3}(\rho g\frac{\partial h}{\partial x})^2 h^3\left[1-\frac{6}{(m+1)(m+2)(m+3)}\right]\\ &+\frac{1}{2}(\rho g)^3\left(h\frac{\partial h}{\partial x}\right)^4\left[1-\frac{24}{(m+1)(m+2)(m+3)(m+4)}\right]\Big\}+u_b\frac{\partial h}{\partial x} \quad .\end{aligned} \tag{B19}$$

Had it been assumed that $A=\bar{A}_2$ in (B2) and (B3) then (B19) would have been

$$\frac{\partial(h\bar{u})}{\partial x}=\bar{A}_2\left[\bar{\sigma}_x'^3 h+\bar{\sigma}_x'^2\rho g\left(h\frac{\partial h}{\partial x}\right)^2+\bar{\sigma}_x'\frac{1}{3}(\rho g\frac{\partial h}{\partial x})^2 h^3+\frac{1}{2}(\rho g)^3\left(h\frac{\partial h}{\partial x}\right)^4\right]+u_b\frac{\partial h}{\partial x} \quad . \tag{B20}$$

Again, no simple relation exists between $\bar{A}_2$ and A_o and m.

Substituting values for East Antarctica and eliminating insignificant terms yields

$$\begin{aligned}\frac{\partial(h\bar{u})}{\partial x}=A_o\Big\{&\bar{\sigma}_x'\frac{1}{3}(\rho g\frac{\partial h}{\partial x})^2 h^3\left[1-\frac{6}{(m+1)(m+2)(m+3)}\right]\\ &+\frac{1}{2}(\rho g)^3\left(h\frac{\partial h}{\partial x}\right)^4\left[1-\frac{24}{(m+1)(m+2)(m+3)(m+4)}\right]\end{aligned} \tag{B21}$$

$$\frac{\partial(h\bar{u})}{\partial x}=\bar{A}_2\left[\bar{\sigma}_x'\frac{1}{3}(\rho g\frac{\partial h}{\partial x})^2 h^3+\frac{1}{2}(\rho g)^3\left(h\frac{\partial h}{\partial x}\right)^4\right]\Big\} \quad . \tag{B22}$$

For m=0.05, (B18) gives $\bar{A}_1 \sim 0.11A_o$, and (B21) and (B22) give $\bar{A}_2$ between

$0.09A_o$ and $0.10A_o$. Thus, the different weighting schemes do not cause large differences in calculated values of $\bar{A}$ in East Antarctica, and it is valid to assume $A=\bar{A}$.

Finally, consider typical ice-stream values (appendix A): h=1000 m; $\frac{\partial h}{\partial x}=-2\times10^{-3}$; $\frac{\partial^2 h}{\partial x^2}=0$, $\frac{\partial \bar{\sigma}'_x}{\partial x}=4.13\times10^{-2}$; $\bar{\sigma}'_x=3.5\times10^4$. Substituting into equations derived from the shear-flow law (B14) and (B15) and simplifying to eliminate insignificant terms gives

$$\bar{A}_1=A_o\left[1-\frac{6}{(m+1)(m+2)(m+3)}\right] \quad . \tag{B23}$$

Substituting into equations derived from the longitudinal flow law (B19) and (B20) and simplifying gives

$$\frac{\partial(h\bar{u})}{\partial x}=A_o\left\{\bar{\sigma}'^3_x h\left[1-\frac{1}{m+1}\right]+\bar{\sigma}'_x\frac{1}{3}(\rho g\frac{\partial h}{\partial x})^2 h^3\left[1-\frac{6}{(m+1)(m+2)(m+3)}\right]\right\} \tag{B24}$$

$$\frac{\partial(h\bar{u})}{\partial x}=\bar{A}_2\left[\bar{\sigma}'^3_x h+\frac{1}{3}\bar{\sigma}'_x(\rho g\frac{\partial h}{\partial x})^2 h^3\right] \tag{B25}$$

and $\bar{A}_2$ is effectively given by

$$A_o\left[1-\frac{1}{m+1}\right]<\bar{A}_2<A_o\left[1-\frac{6}{(m+1)(m+2)(m+3)}\right] \quad . \tag{B26}$$

Comparison of (B23) and (B26) for m=0.05 shows that the two weighting schemes do not lead to significantly different values of $\bar{A}$. Thus, it is valid to take $A=\bar{A}$ both in shear-dominated ice sheets and in ice streams.

Appendix C. Depth-variation of longitudinal-deviatoric stress.

Longitudinal-deviatoric stress varies both vertically and horizontally in an ice sheet. In the derivation of model equations (page 9) it was assumed that the longitudinal-deviatoric stress can be replaced by a weighted average over depth that varies only horizontally. Substitution of a weighted average over depth for a depth-varying parameter is a commonly-used device in glaciological calculations, especially for the flow-law parameter (Paterson, 1981, p. 83-84). The following calculations demonstrate that depth-dependence of longitudinal-deviatoric stress is relatively weak at those depths where most deformation occurs, so that longitudinal-deviatoric stress is especially suited for replacement by a weighted average over depth.

Ci. East Antarctica downglacier from Dome C.

Along a flow line from Dome C to the coast in East Antarctica, longitudinal-deviatoric stress varies only slowly with depth in the lower third of the ice sheet where most deformation occurs. This result is obtained by using published models to calculate vertical strain rates, temperatures and hence flow-law parameters, and shear stresses as functions of depth, and then solving the flow-law equation for stretching to find the longitudinal-deviatoric stress as a function of depth.

Vertical-strain-rate models are discussed in Bolzan (1984). He considers

$$\dot{\varepsilon}_z = -\frac{b(n+1)}{h\ n}\left[1-\left(\frac{h-z}{h}\right)^n\right] \qquad (C1)$$

$$\dot{\varepsilon}_z = -\frac{b}{h}(n+1)\left[1-\left(\frac{h-z}{h}\right)\right]^n \qquad (C2)$$

which he designates class I and class II flow, respectively. Near Dome C he finds that best fits are obtained with n between 0 and 1 for class I models, and n equal to approximately 2 for class II models. Models considered here include class I models with n=0.5 and with n=1 (linear variation of vertical strain rate with depth) and class II models with n=0 (constant vertical strain rate with depth) and with n=2. Although depth-variation of vertical strain rate is not well-understood, it is probable that this range of models encompasses actual behavior. For two-dimensional flow of incompressible ice,

vertical strain rate is related to horizontal strain rate by the simple formula

$$\dot{\varepsilon}_x = -\dot{\varepsilon}_z \quad . \tag{C3}$$

Because the flow-law parameter varies with temperature, it is necessary to calculate temperature profiles. Temperature in an ice sheet depends on such factors as geothermal heat flow, basal-melting rate, surface temperature, internal-heat generation, thermal properties of ice, and both horizontal and vertical advection. Many of these factors are not well-constrained or are difficult to calculate.

One temperature model that combines reasonable accuracy and simple calculations is the Robin model (Robin, 1955; Clarke and others, 1977). It allows for conduction and vertical advection (class II flow, n=0), but not for horizontal advection. Input data are accumulation rate, ice-sheet thickness, geothermal heat flux (taken to be $5.7 \times 10^{-2} Wm^{-2}$, the value recommended for Dome C by Bolzan, 1984), thermal conductivity of ice ($2.51 Wm^{-2}$), and the temperature at one depth (taken to be the pressure-melting temperature at the bed). The model then yields temperature as a function of depth, which can be read easily from the nondimensional graphs in Clarke and others (1977).

It is recognized that each vertical-strain-rate model should have its own temperature profile. Considering the magnitude of other probable errors involved, this would introduce significant

calculational complications without significantly improving the quality of results.

The flow-law parameter, A, exhibits an Arrhenius-type temperature dependence with different rate constants above and below -10 °C. To good approximation

$$A(T)=5.3\times10^{-24}\exp(0.23216T),\ 0\geq T\geq -10\ ^{o}C \qquad (C4)$$

$$A(T)=1.7785\times10^{-24}\exp(0.12297T),\ -10\geq T\geq -50\ ^{o}C \qquad (C5)$$

where T is temperature in degrees Celsius (Paterson, 1981, p.39).

Shear stress is calculated from ice-sheet thickness and surface slope according to equation (3). Calculated values of A, $\dot{\varepsilon}_x$, and τ_{xz} are then substituted into the longitudinal-flow-law equation (1), which is solved for longitudinal-deviatoric stress. Results for three positions along a flow line from Dome C to the coast are shown in figures C1-C3, and in tables CI-CIII.

It is apparent that longitudinal-deviatoric stress does vary with depth. This variation, however, is relatively weaker near the bed, where most deformation occurs, than it is farther from the bed. Only 25 km from the ice divide, shear stress varies more rapidly with depth than longitudinal-deviatoric stress in the lower two-tenths of the ice sheet for most models considered. Farther from the ice divide, depth-variation of shear stress is larger than depth-variation of longitudinal-deviatoric stress in the lower third of the ice sheet for all models considered.

Figures C1, C2, and C3. Depth-variation of longitudinal-deviatoric stress (σ'_x), for different vertical-strain-rate models from Bolzan (1984). Models used are Bolzan's class I with n=0.5 and n=1, and class II with n=0 and n=2. Shear stress (τ_{xz}) is also shown as a function of depth, calculated according to equation (3). Figures C1, C2, and C3 are plots of values from tables CI, CII, and CIII, respectively, and represent positions 25 km, 400 km, and 715 km downglacier from Dome C, respectively.

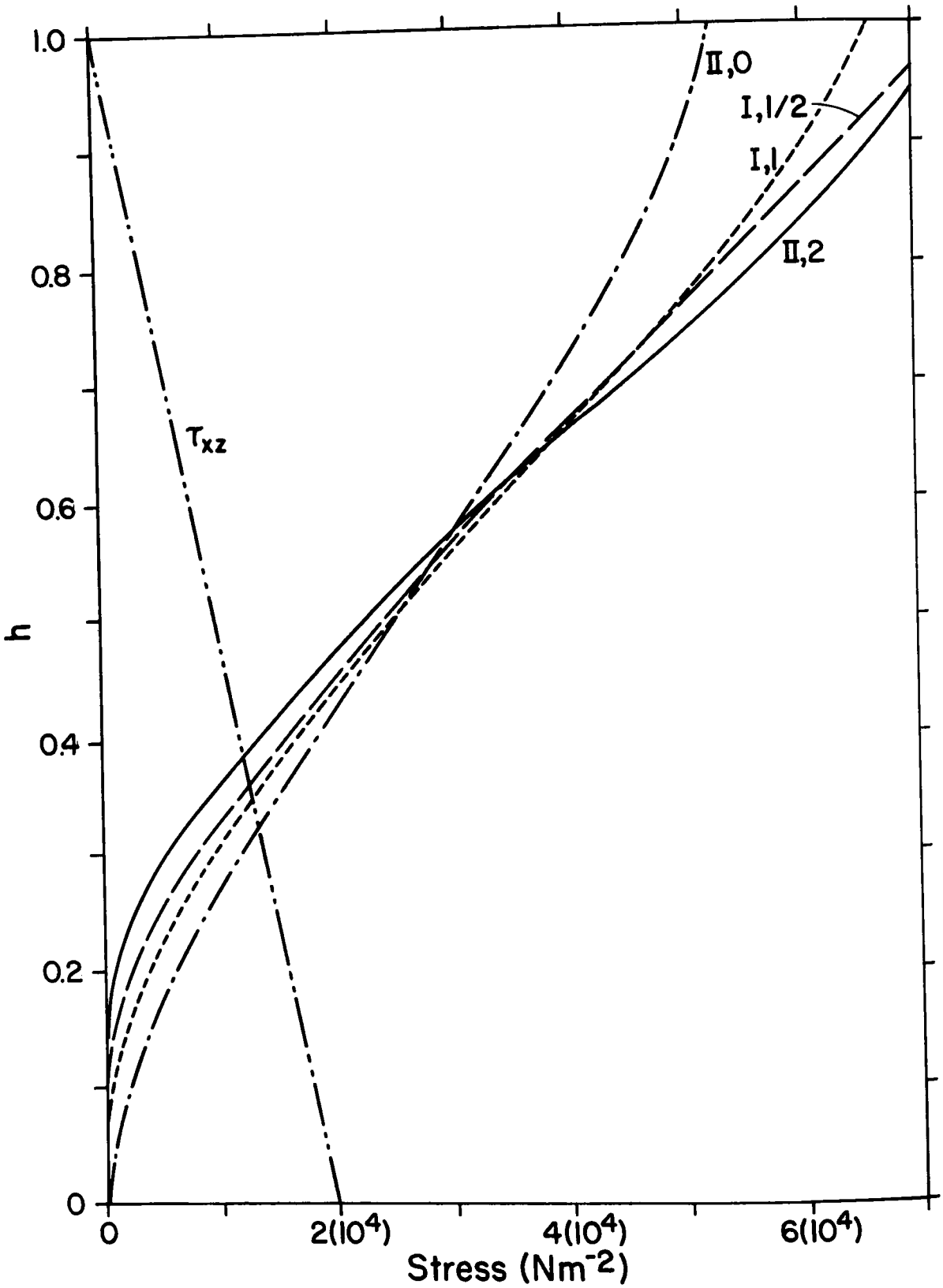
1.0
0.8
0.6
0.4
0.2
0
h
II,0
I,1/2
I,1
II,2
τ_{xz}
0
2(10^4)
4(10^4)
6(10^4)
Stress (Nm^-2)

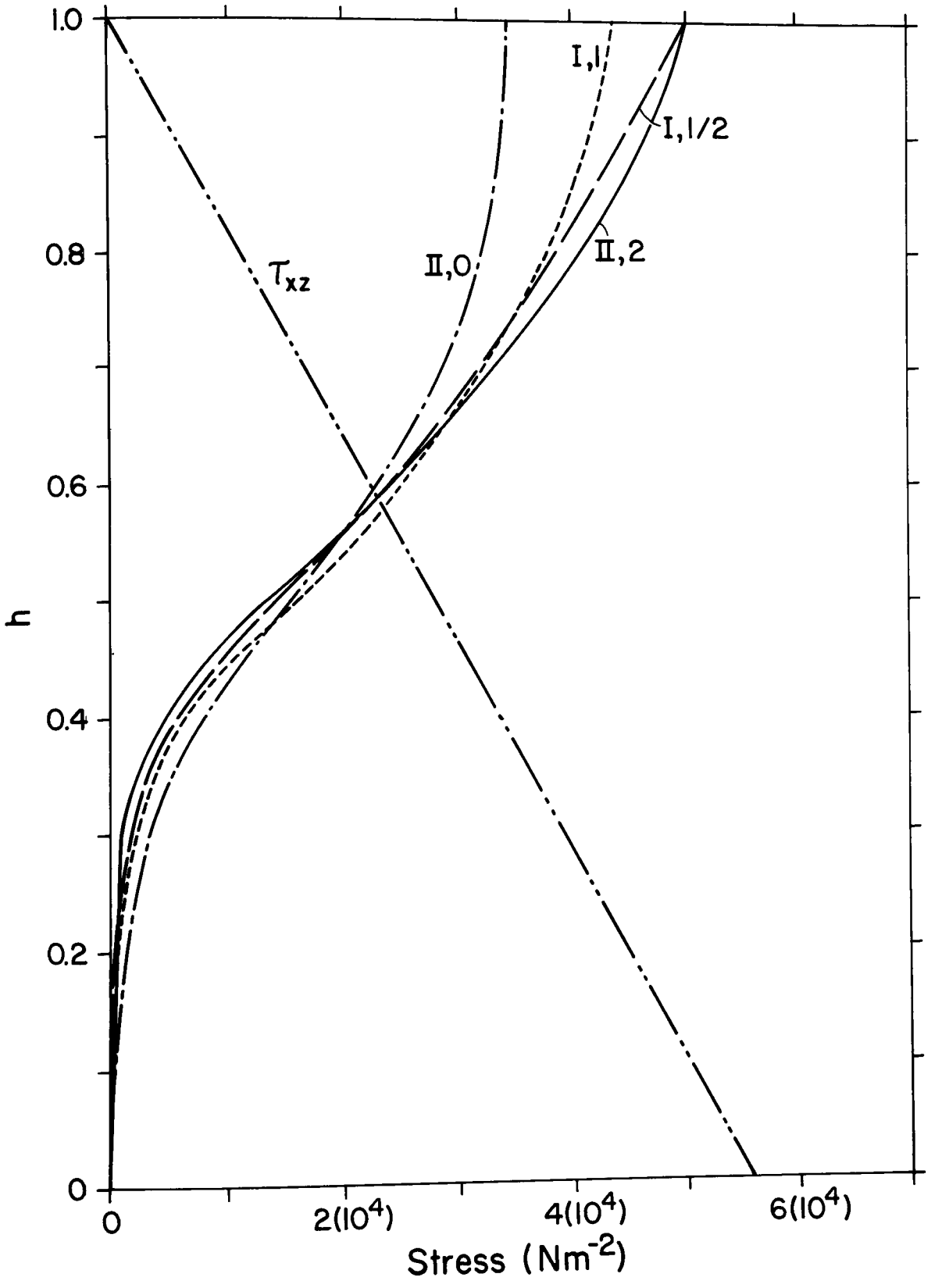
1.0
0.8
0.6
0.4
0.2
0
h
0
2(10^4)
4(10^4)
6(10^4)
Stress (Nm^-2)
τxz
II,0
I,1
I,1/2
II,2

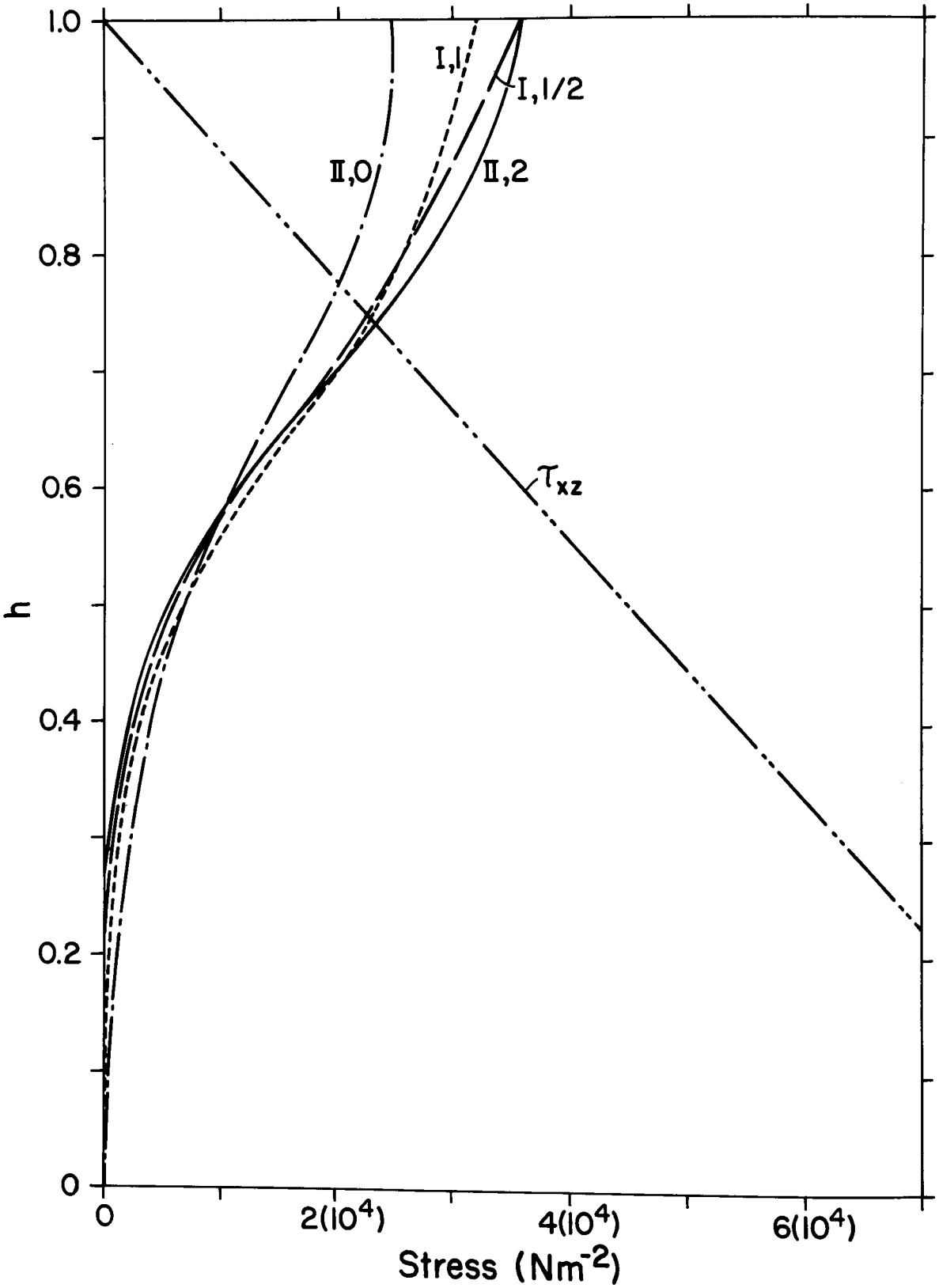
1.0
0.8
0.6
0.4
0.2
0
h
I,1
I,1/2
II,0
II,2
τ_{xz}
0
2(10^4)
4(10^4)
6(10^4)
Stress (Nm^-2)

Table CI. Calculation of longitudinal-deviatoric stress as a function of depth, 25 km from Dome C.

$h=3500m$, $\frac{\partial h}{\partial x}=-6.39\times10^{-4}$, $\dot{b}=1.17\times10^{-9} ms^{-1}$

					class II,n=2
z(m)	T(^{o}C)	A[$(Nm^{-2})^{-3}s^{-1}$]	$\tau_{xz}(Nm^{-2})$	$\dot{\varepsilon}_x(s^{-1})$	$\sigma'_x(Nm^{-2})$
1.0h	-54.3	2.24×10^{-27}	$0.00\times10^{+0}$	1.00×10^{-12}	$7.64\times10^{+4}$
0.9h	-52.7	2.73×10^{-27}	$5.60\times10^{+3}$	8.12×10^{-13}	$6.67\times10^{+4}$
0.8h	-50.3	3.66×10^{-27}	$1.12\times10^{+4}$	6.42×10^{-13}	$5.59\times10^{+4}$
0.7h	-47.1	5.43×10^{-27}	$1.68\times10^{+4}$	4.91×10^{-13}	$4.46\times10^{+4}$
0.6h	-42.3	9.80×10^{-26}	$2.24\times10^{+4}$	3.61×10^{-13}	$3.26\times10^{+4}$
0.5h	-37.6	1.75×10^{-26}	$2.80\times10^{+4}$	2.51×10^{-13}	$2.29\times10^{+4}$
0.4h	-32.0	3.48×10^{-26}	$3.36\times10^{+4}$	1.60×10^{-14}	$1.38\times10^{+3}$
0.3h	-25.6	7.64×10^{-26}	$3.92\times10^{+4}$	9.03×10^{-14}	$5.28\times10^{+2}$
0.2h	-18.5	1.83×10^{-25}	$4.48\times10^{+4}$	4.01×10^{-14}	$8.54\times10^{+2}$
0.1h	-10.5	4.89×10^{-25}	$5.04\times10^{+4}$	1.00×10^{-14}	$6.31\times10^{+1}$
0.0h	-2.6	2.90×10^{-24}	$5.60\times10^{+4}$	$0.00\times10^{+0}$	$0.00\times10^{+0}$

	Class II,n=0		Class I, n=0.5		Class I, n=1	
z(m)	$\dot{\varepsilon}_x(s^{-1})$	$\sigma'_x(Nm^{-2})$	$\dot{\varepsilon}_x(s^{-1})$	$\sigma'_x(Nm^{-2})$	$\dot{\varepsilon}x(s^{-1})$	$\sigma'_x(Nm^{-2})$
1.0h	3.34×10^{-13}	$5.30\times10^{+4}$	1.00×10^{-12}	$7.65\times10^{+4}$	6.69×10^{-13}	$6.68\times10^{+4}$
0.9h	3.34×10^{-13}	$4.96\times10^{+4}$	6.86×10^{-13}	$6.31\times10^{+4}$	6.02×10^{-13}	$6.04\times10^{+4}$
0.8h	3.34×10^{-13}	$4.49\times10^{+4}$	5.55×10^{-13}	$5.32\times10^{+4}$	5.35×10^{-13}	$5.26\times10^{+4}$
0.7h	3.34×10^{-13}	$3.92\times10^{+4}$	4.53×10^{-13}	$4.34\times10^{+4}$	4.68×10^{-13}	$4.39\times10^{+4}$
0.6h	3.34×10^{-13}	$3.18\times10^{+4}$	3.69×10^{-13}	$3.29\times10^{+4}$	4.01×10^{-13}	$3.38\times10^{+4}$
0.5h	3.34×10^{-13}	$2.55\times10^{+4}$	2.94×10^{-13}	$2.43\times10^{+4}$	3.34×10^{-13}	$2.55\times10^{+4}$
0.4h	3.34×10^{-13}	$1.90\times10^{+4}$	2.27×10^{-13}	$1.61\times10^{+3}$	2.67×10^{-13}	$1.73\times10^{+3}$
0.3h	3.34×10^{-13}	$1.25\times10^{+4}$	1.63×10^{-13}	$8.14\times10^{+3}$	2.01×10^{-13}	$9.31\times10^{+3}$
0.2h	3.34×10^{-13}	$6.20\times10^{+3}$	1.06×10^{-13}	$2.22\times10^{+3}$	1.34×10^{-14}	$2.78\times10^{+2}$
0.1h	3.34×10^{-13}	$2.08\times10^{+1}$	$5.11\times10^{+0}$	$3.27\times10^{+2}$	$6.69\times10^{+0}$	$4.25\times10^{+0}$
0.0h	3.34×10^{-13}	$3.67\times10^{+1}$	$0.0o\times10^{+0}$	$0.00\times10^{+0}$	$0.00\times10^{+0}$	$0.00\times10^{+0}$

Table CII. Calculation of longitudinal-deviatoric stress as a function of depth, 400 km from Dome C.

$h=2950m$, $\frac{\partial h}{\partial x}=-2.13\times10^{-3}$, $\dot{b}=2.13\times10^{-9} ms^{-1}$

				class II,n=2	
z(m)	T(^{o}C)	A[$(Nm^{-2})^{-3}s^{-1}$]	$\tau_{xz}(Nm^{-2})$	$\dot{\varepsilon}_x(s^{-1})$	$\sigma'_x(Nm^{-2})$
1.0h	-37.7	1.72×10^{-26}	$0.00\times10^{+0}$	2.17×10^{-12}	$5.02\times10^{+4}$
0.9h	-37.7	1.72×10^{-26}	$5.60\times10^{+3}$	1.75×10^{-12}	$4.65\times10^{+4}$
0.8h	-36.4	2.02×10^{-26}	$1.12\times10^{+4}$	1.39×10^{-12}	$4.00\times10^{+4}$
0.7h	-35.0	2.40×10^{-26}	$1.68\times10^{+4}$	1.06×10^{-12}	$3.27\times10^{+4}$
0.6h	-33.0	3.07×10^{-26}	$2.24\times10^{+4}$	7.80×10^{-13}	$2.38\times10^{+4}$
0.5h	-30.3	4.28×10^{-26}	$2.80\times10^{+4}$	5.42×10^{-13}	$1.32\times10^{+4}$
0.4h	-25.6	7.64×10^{-26}	$3.36\times10^{+4}$	3.47×10^{-13}	$3.97\times10^{+3}$
0.3h	-20.3	1.47×10^{-25}	$3.92\times10^{+4}$	1.95×10^{-13}	$8.63\times10^{+2}$
0.2h	-14.8	2.85×10^{-25}	$4.48\times10^{+4}$	8.66×10^{-14}	$1.51\times10^{+2}$
0.1h	-8.9	6.71×10^{-24}	$5.04\times10^{+4}$	2.17×10^{-14}	$1.27\times10^{+1}$
0.0h	-2.2	3.18×10^{-24}	$5.60\times10^{+4}$	$0.00\times10^{+0}$	$0.00\times10^{+0}$

	Class II,n=0		Class I, n=0.5		Class I, n=1	
z(m)	$\dot{\varepsilon}_x(s^{-1})$	$\sigma'_x(Nm^{-2})$	$\dot{\varepsilon}_x(s^{-1})$	$\sigma'_x(Nm^{-2})$	$\dot{\varepsilon}_x(s^{-1})$	$\sigma'_x(Nm^{-2})$
1.0h	7.22×10^{-13}	$3.48\times10^{+4}$	2.17×10^{-12}	$5.02\times10^{+4}$	1.44×10^{-12}	$4.37\times10^{+4}$
0.9h	7.22×10^{-13}	$3.45\times10^{+4}$	1.48×10^{-12}	$4.39\times10^{+4}$	1.30×10^{-12}	$4.20\times10^{+4}$
0.8h	7.22×10^{-13}	$3.16\times10^{+4}$	1.20×10^{-12}	$3.79\times10^{+4}$	1.16×10^{-12}	$3.74\times10^{+4}$
0.7h	7.22×10^{-13}	$2.81\times10^{+4}$	9.80×10^{-13}	$3.21\times10^{+4}$	1.01×10^{-12}	$3.21\times10^{+4}$
0.6h	7.22×10^{-13}	$2.29\times10^{+4}$	7.96×10^{-13}	$2.40\times10^{+4}$	8.66×10^{-13}	$2.50\times10^{+4}$
0.5h	7.22×10^{-13}	$1.61\times10^{+4}$	6.34×10^{-13}	$1.48\times10^{+4}$	7.22×10^{-13}	$1.61\times10^{+4}$
0.4h	7.22×10^{-13}	$7.93\times10^{+3}$	4.88×10^{-13}	$5.51\times10^{+3}$	5.78×10^{-13}	$6.46\times10^{+3}$
0.3h	7.22×10^{-13}	$3.18\times10^{+3}$	3.54×10^{-13}	$1.56\times10^{+3}$	4.33×10^{-13}	$1.91\times10^{+3}$
0.2h	7.22×10^{-13}	$1.26\times10^{+3}$	2.29×10^{-13}	$4.00\times10^{+2}$	2.89×10^{-13}	$5.05\times10^{+2}$
0.1h	7.22×10^{-13}	$4.24\times10^{+2}$	1.11×10^{-13}	$6.51\times10^{+1}$	1.44×10^{-13}	$8.45\times10^{+1}$
0.0h	7.22×10^{-13}	$7.24\times10^{+1}$	$0.00\times10^{+0}$	$0.00\times10^{+0}$	$0.00\times10^{+0}$	$0.00\times10^{+0}$

Table CIII. Calculation of longitudinal-deviatoric stress as a function of depth, 715 km from Dome C.

$h=1935m$, $\frac{\partial h}{\partial x}=-5.22\times10^{-3}$, $\dot{b}=5,93\times10^{-9}ms^{-1}$

				class II,n=2	
z(m)	T(°C)	$A[(Nm^{-2})^{-3}s^{-1}]$	$\tau_{xz}(Nm^{-2})$	$\dot{\varepsilon}_x(s^{-1})$	$\sigma'_x(Nm^{-2})$
1.0h	-18.1	1.92×10^{-25}	$0.00\times10^{+0}$	9.19×10^{-12}	$3.63\times10^{+4}$
0.9h	-18.1	1.92×10^{-25}	$9.01\times10^{+3}$	7.45×10^{-12}	$3.31\times10^{+4}$
0.8h	-18.1	1.92×10^{-25}	$1.80\times10^{+4}$	5.88×10^{-12}	$2.79\times10^{+4}$
0.7h	-18.0	1.94×10^{-25}	$2.70\times10^{+4}$	4.50×10^{-12}	$2.03\times10^{+4}$
0.6h	-17.7	2.02×10^{-25}	$3.60\times10^{+4}$	3.31×10^{-12}	$1.15\times10^{+4}$
0.5h	-16.9	2.23×10^{-25}	$4.50\times10^{+4}$	2.30×10^{-12}	$5.03\times10^{+3}$
0.4h	-15.2	2.74×10^{-25}	$5.40\times10^{+4}$	1.47×10^{-12}	$1.84\times10^{+3}$
0.3h	-12.6	3.78×10^{-25}	$6.31\times10^{+4}$	8.27×10^{-13}	$5.49\times10^{+2}$
0.2h	-9.4	5.98×10^{-24}	$7.21\times10^{+4}$	3.68×10^{-13}	$1.18\times10^{+2}$
0.1h	-5.4	1.51×10^{-24}	$8.11\times10^{+4}$	9.19×10^{-14}	$9.25\times10^{+0}$
0.0h	-1.4	3.83×10^{-24}	$9.01\times10^{+4}$	$0.00\times10^{+0}$	$0.00\times10^{+0}$

	Class II,n=0		Class I, n=0.5		Class I, n=1	
z(m)	$\dot{\varepsilon}_x(s^{-1})$	$\sigma'_x(Nm^{-2})$	$\dot{\varepsilon}_x(s^{-1})$	$\sigma'_x(Nm^{-2})$	$\dot{\varepsilon}_x(s^{-1})$	$\sigma'_x(Nm^{-2})$
1.0h	3.06×10^{-12}	$2.52\times10^{+4}$	9.19×10^{-12}	$3.63\times10^{+4}$	6.13×10^{-12}	$3.17\times10^{+4}$
0.9h	3.06×10^{-12}	$2.41\times10^{+4}$	6.28×10^{-12}	$3.11\times10^{+4}$	5.52×10^{-12}	$2.98\times10^{+4}$
0.8h	3.06×10^{-12}	$2.09\times10^{+4}$	5.08×10^{-12}	$2.62\times10^{+4}$	4.90×10^{-12}	$2.58\times10^{+4}$
0.7h	3.06×10^{-12}	$1.61\times10^{+4}$	4.16×10^{-12}	$1.94\times10^{+4}$	4.29×10^{-12}	$1.98\times10^{+4}$
0.6h	3.06×10^{-12}	$1.07\times10^{+4}$	3.38×10^{-12}	$1.17\times10^{+4}$	3.68×10^{-12}	$1.25\times10^{+4}$
0.5h	3.06×10^{-12}	$6.63\times10^{+3}$	2.69×10^{-12}	$5.86\times10^{+3}$	3.06×10^{-12}	$6.63\times10^{+3}$
0.4h	3.06×10^{-12}	$3.81\times10^{+3}$	2.07×10^{-12}	$2.58\times10^{+3}$	2.45×10^{-12}	$3.06\times10^{+3}$
0.3h	3.06×10^{-12}	$2.03\times10^{+2}$	1.50×10^{-13}	$7.96\times10^{+2}$	1.84×10^{-12}	$1.22\times10^{+2}$
0.2h	3.06×10^{-12}	$9.84\times10^{+2}$	9.71×10^{-13}	$3.12\times10^{+2}$	1.23×10^{-13}	$3.96\times10^{+1}$
0.1h	3.06×10^{-12}	$3.08\times10^{+2}$	4.72×10^{-13}	$4.75\times10^{+1}$	$6.13\times10^{+0}$	$6.17\times10^{+0}$
0.0h	3.06×10^{-12}	$9.84\times10^{+1}$	$0.00\times10^{+0}$	$0.00\times10^{+0}$	$0.00\times10^{+0}$	$0.00\times10^{+0}$

Cii. West Antarctic ice streams.

Longitudinal-deviatoric stresses do not tend to zero at the bed of an ice stream as they do at the bed of an ice sheet with no basal sliding. This complicates the calculation of longitudinal-deviatoric stresses in ice streams, and a different computational scheme from that used in Ci, above, must be devised. The method adopted here is to require mass balance at two points separated by a small distance, Δx, calculate horizontal velocity as a function of depth in a finite-difference approximation at each point, and from this calculate $\frac{\Delta u}{\Delta x}$, which is the finite-difference approximation of the longitudinal strain rate, $\dot{\varepsilon}_x$.

Consider the ice stream described in Appendices A and B. Flow-law parameters and shear stresses are calculated as in Ci, assuming that longitudinal variations in the flow-law parameter and in the longitudinal-deviatoric stress are small and can be ignored.

Total horizontal velocity, u, is the sum of sliding velocity, u_b, and deformational velocity, u_d. Deformational velocity is calculated by finite-difference integration of equation (2) over depth, with $\sigma'_x = \bar{\sigma}'_x$ in each interval. Initially $\bar{\sigma}'_x$ is taken to be $3.25 \times 10^4 \text{Nm}^{-2}$ in each interval; this is then varied in subsequent iterations.

After deformational velocity is calculated, bottom-sliding velocity is chosen to maintain mass balance, and total velocity is calculated as a function of depth for the two points along the flow line that are under consideration. It is then straightforward to calculate $\frac{\Delta u}{\Delta x} = \dot{\varepsilon}_x$, and then σ'_x from equation (1). Using the new

values of σ'_x, the entire calculation is then repeated iteratively until values of σ'_x from successive iterations do not change. In practice, only one iteration is required.

Results are shown in figure C4. Values of longitudinal-deviatoric stress are seen to vary by only a factor of three over the ice-stream thickness; most of this variation is caused by increased resistance to deformation of colder ice near the surface.

It is apparent that longitudinal-deviatoric stress varies with depth both in shear-dominated regions of the East Antarctic ice sheet and in ice streams. Such variation is not extreme, however, especially throughout ice streams and in deep regions of shear-dominated ice sheets where most deformation occurs. Depth-variation of the flow-law parameter (which frequently is replaced by a weighted average over depth) and of the shear stress (which seldom is replaced by a weighted average over depth) are usually larger that depth-variation of longitudinal-deviatoric stress. Thus, it is reasonable to replace the longitudinal-deviatoric stress with a weighted average over depth.

There are actually two different weighting schemes for longitudinal-deviatoric stress, just as there are for the flow-law parameter (Appendix B). As in Appendix B, both schemes give greatest weight to deep layers where deformation is fastest, and thus give similar values for the depth-averaged-longitudinal-deviatoric stress.

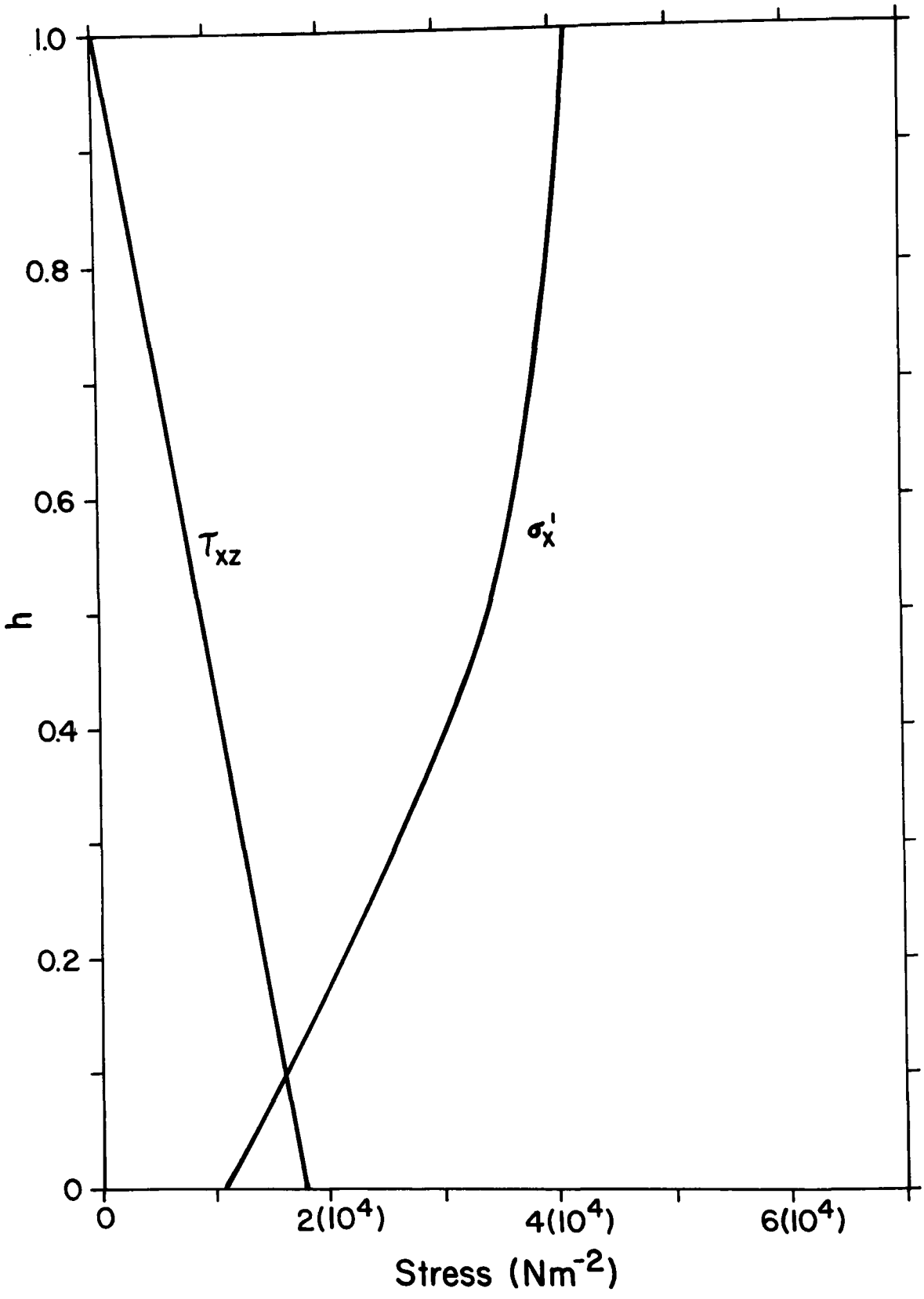

Figure C4. Depth-variation of longitudinal-deviatoric (σ') and shear (τ_{xz}) stresses for an ice stream. Values plotted are calculated in table CIV.

Table CIV. Calculation of longitudinal-deviatoric stress as a function of depth in an ice stream.

$h=1000m$, $\frac{\partial h}{\partial x}=-0.002$, $b=4.75\times10^{-9}ms^{-1}$, $\Delta x=1000m$

$u_e(x=x_o)=7.92\times10^{-6}ms^{-1}$, $u_e(x=x_o+\Delta x)=7.94063\times10^{-6}ms^{-1}$

i	z_i	T(°C)	$\bar{A}_i[(Nm^{-2})^{-3}s^{-1}]$	$\tau_{xz}(Nm^{-2})$
10	0.95h	-14.3	3.07×10^{-25}	$0.00\times10^{+0}$
9	0.85h	-14.0	3.20×10^{-25}	$2.68\times10^{+3}$
8	0.75h	-13.4	3.45×10^{-25}	$4.46\times10^{+3}$
7	0.65h	-12.5	3.86×10^{-25}	$6.24\times10^{+3}$
6	0.55h	-11.4	4.42×10^{-25}	$8.03\times10^{+3}$
5	0.45h	-10.0	5.49×10^{-25}	$9.81\times10^{+3}$
4	0.35h	-8.3	7.89×10^{-25}	$1.16\times10^{+4}$
3	0.25h	-6.4	1.25×10^{-24}	$1.34\times10^{+4}$
2	0.15h	-4.3	2.01×10^{-24}	$1.52\times10^{+4}$
1	0.05h	-2.2	3.33×10^{-24}	$1.70\times10^{+4}$

	$x=x_o$	$x=x_o+\Delta x$		
i	$\bar{u}_{id}(ms^{-1})$	$\bar{u}_{id}(ms^{-1})$	$\dot{\varepsilon}_x(s^{-1})$	$\bar{\sigma}'_{xi}(Nm^{-2})$
10	3.24132×10^{-8}	3.23014×10^{-8}	2.061×10^{-11}	$4.06\times10^{+4}$
9	3.22933×10^{-8}	3.21838×10^{-8}	2.061×10^{-11}	$4.00\times10^{+4}$
8	3.20367×10^{-8}	3.19299×10^{-8}	2.061×10^{-11}	$3.89\times10^{+4}$
7	3.16072×10^{-8}	3.15034×10^{-8}	2.062×10^{-11}	$3.73\times10^{+4}$
6	3.09457×10^{-8}	3.08459×10^{-8}	2.062×10^{-11}	$3.54\times10^{+4}$
5	2.99275×10^{-8}	2.98318×10^{-8}	2.062×10^{-11}	$3.25\times10^{+4}$
4	2.82177×10^{-8}	2.81288×10^{-8}	2.063×10^{-11}	$2.82\times10^{+4}$
3	2.50632×10^{-8}	2.49855×10^{-8}	2.064×10^{-11}	$2.31\times10^{+4}$
2	1.90787×10^{-8}	1.90206×10^{-9}	2.066×10^{-11}	$1.82\times10^{+4}$
1	7.57980×10^{-9}	7.55700×10^{-9}	2.070×10^{-11}	$1.33\times10^{+4}$

$\bar{u}_d=2.69163\times10^{-8}$ $\bar{u}_d=2.68288\times10^{-8}$

Appendix D. Demonstration that bottom sliding is unimportant in East Antarctica.

In applying the model to East Antarctica, it was assumed that no bottom sliding occurs. Radio-echo sounding has shown, however, that some portions of the bed under the East Antarctic ice sheet are at the basal-melting temperature (Oswald and Robin, 1973) and free to slide.

Small amounts of basal sliding will not invalidate the results obtained in this study for East Antarctica, because of the empirical way in which the flow-law parameter, $\bar{A}$, is calculated. If basal sliding is assumed to be zero but some basal sliding actually occurs, calculated values of $\bar{A}$ will be larger (corresponding to "softer" ice that deforms more easily) than ice-sheet temperature would justify. In nonsteady flow, the model ice sheet will respond as a soft ice sheet moving entirely by internal deformation, rather than as a harder ice sheet with some basal sliding. Because increased stress increases ice flux both in a soft ice sheet with no basal sliding and in a harder ice sheet with basal sliding, small amounts of basal sliding may be modelled as internal deformation without introducing large errors; however, because basal sliding does not obey the same flow law as internal deformation, basal sliding must be modelled explicitly if it becomes rapid.

To assess the importance of basal sliding in East Antarctica, it is necessary to calculate deformational ice fluxes and compare with balance fluxes. If close agreement is obtained, then basal sliding is

not important. If balance fluxes significantly exceed fluxes due to internal deformation, then basal sliding is important.

The rate of ice deformation at a point depends on the longitudinal and shear stresses, and depends on the flow-law parameter, which varies with temperature. Shear stress can be calculated from ice-sheet configuration according to equation (3). Depth-dependence of temperature, temperature-dependence of the flow-law parameter, and then longitudinal stress are calculated as in Appendix C, assuming class I flow with n=0.5.

To calculate deformational velocities, the ice column is divided into n discrete intervals of length Δz_i (here n=10, Δz_i=0.1h). For each interval, midpoint values ($z=z_i$) are calculated for the flow-law parameter, A_i, longitudinal-deviatoric stress, σ'_{xi}, and shear stress, τ_{xzi}, and these are assumed to represent averages over the i^{th} interval. Change in horizontal velocity across an interval, Δu_i, is then given by the discrete version of the shear flow law

$$\Delta u_i = 2\bar{A}_i \Delta z_i \left[\left(\rho g \frac{\partial h}{\partial x}\right)^3 (h^3 - 3h^2 z_i + 3h z_i^2 - z_i^3) + \left(\rho g \frac{\partial h}{\partial x}\right) \bar{\sigma}'^2_x (h - z_i) \right] \quad . \tag{D1}$$

The deformational velocity at the top of the j^{th} interval, where the base of the interval j=1 is in contact with the bed, is

$$u_j = \sum_{i=1}^{j} \Delta u_i \quad . \tag{D2}$$

The mean deformational velocity in the $(j+1)^{st}$ interval is

$$\bar{u}_{j+1} = u_j + \frac{1}{2} \Delta u_{j+1} \tag{D3}$$

and the total ice flux due to deformation, $(\overline{hu})_d$, is

$$(\overline{hu})_d = \sum_{j=1}^{n} \overline{u}_j \Delta z_i . \qquad \text{(D4)}$$

The balance or equilibrium ice flux, $(\overline{hu})_e$, is obtained by integrating the accumulation-rate profile (36) from the ice divide to yield

$$(\overline{hu})_e = 1.15\times10^{+3}[\exp(4.70\times10^{-6}x)-1]+3.16\times10^{-2}x \text{ m}^2\text{a}^{-1}. \qquad \text{(D5)}$$

Calculated values of $(\overline{hu})_d$ and $(\overline{hu})_e$ for three points along a flow line from Dome C to the coast are shown in tables DI, DII, and DIII. Basal sliding is calculated to account for 15 percent to 23 percent of total ice flux.

Several of the assumptions used in this calculation may introduce significant errors. The vertical strain rate probably differs from the assumed model. Calculated temperature profiles ignore horizontal advection and internal heat generation, and are based on values of geothermal heat flow that are poorly constrained. Published estimates of the flow-law parameter for a given temperature differ by up to an order of magnitude from those used here (Paterson, 1981, p. 34-40). Values of the flow-law parameter assumed here do not explicitly consider fabric development, which can have major effects on ice flow. The assumed accumulation-rate profile probably includes significant errors. The ice sheet does not have a precisely horizontal bed nor an exact Vialov (1958) profile, and it probably is not in steady state.

It is difficult to estimate the magnitude of these probable errors. Ice velocity of about 20ma^{-1} generates as much heat

Table DI. Calculation of deformational and balance velocities 25 km from Dome C.

Position, ice thickness, surface slope, accumulation rate, and profiles of temperature, flow-law parameter, shear stress, vertical strain rate (class I, n=0.5), and longitudinal-deviatoric stress are the same as in table CI.

i	z_i	$\Delta u_i (ms^{-1})$	$\bar{u}_i (ms^{-1})$	$\bar{u}_i \Delta z_i (m^2 s^{-1})$
10	0.95h	8.007×10^{-12}	7.575×10^{-9}	2.651×10^{-6}
9	0.85h	2.268×10^{-11}	7.571×10^{-9}	2.650×10^{-6}
8	0.75h	3.644×10^{-11}	7.530×10^{-9}	2.636×10^{-6}
7	0.65h	5.285×10^{-11}	7.485×10^{-9}	2.620×10^{-6}
6	0.55h	7.301×10^{-11}	7.423×10^{-9}	2.598×10^{-6}
5	0.45h	1.013×10^{-10}	7.336×10^{-9}	2.567×10^{-6}
4	0.35h	1.456×10^{-10}	7.219×10^{-9}	2.524×10^{-6}
3	0.25h	6.329×10^{-10}	6.822×10^{-9}	2.388×10^{-6}
2	0.15h	1.012×10^{-9}	6.000×10^{-9}	2.100×10^{-6}
1	0.05h	5.494×10^{-9}	2.747×10^{-9}	9.615×10^{-7}

$(h\bar{u})_d = 2.370 \times 10^{-5}$

$(h\bar{u})_e = 2.957 \times 10^{-5}$

$[(h\bar{u})_e - (h\bar{u})_d]/(h\bar{u})_d = 19.8\%$

Table DII. Calculation of deformational and balance velocities 400 km from Dome C.

Position, ice thickness, surface slope, accumulation rate, and profiles of temperature, flow-law parameter, shear stress, vertical strain rate (class I, n=0.5), and longitudinal-deviatoric stress are the same as in table CII.

i	z_i	$\Delta u_i (ms^{-1})$	$\bar{u}_i (ms^{-1})$	$\bar{u}_i \Delta z_i (m^2 s^{-1})$
10	0.95h	6.038×10^{-11}	1.733×10^{-7}	5.113×10^{-5}
9	0.85h	1.618×10^{-10}	1.733×10^{-7}	5.112×10^{-5}
8	0.75h	2.571×10^{-10}	1.730×10^{-7}	5.104×10^{-5}
7	0.65h	3.723×10^{-10}	1.727×10^{-7}	5.094×10^{-5}
6	0.55h	5.457×10^{-10}	1.723×10^{-7}	5.082×10^{-5}
5	0.45h	1.110×10^{-9}	1.715×10^{-7}	5.058×10^{-5}
4	0.35h	3.014×10^{-9}	1.694×10^{-7}	4.998×10^{-5}
3	0.25h	8.938×10^{-9}	1.634×10^{-7}	4.819×10^{-5}
2	0.15h	2.722×10^{-8}	1.453×10^{-7}	4.287×10^{-5}
1	0.05h	1.317×10^{-7}	6.586×10^{-8}	1.943×10^{-5}

$$(h\bar{u})_d = 4.661 \times 10^{-4}$$

$$(h\bar{u})_e = 6.028 \times 10^{-4}$$

$$[(h\bar{u})_e - (h\bar{u})_d]/(h\bar{u})_d = 22.7\%$$

Table DIII. Calculation of deformational and balance velocities 715 km from Dome C.

Position, ice thickness, surface slope, accumulation rate, and profiles of temperature, flow-law parameter, shear stress, vertical strain rate (class I, n=0.5), and longitudinal-deviatoric stress are the same as in Table CIII.

i	z_i	$\Delta u_i (ms^{-1})$	$\bar{u}_i (ms^{-1})$	$\bar{u}_i \Delta z_i (m^2 s^{-1})$
10	0.95h	3.757×10^{-10}	8.702×10^{-7}	1.684×10^{-4}
9	0.85h	7.190×10^{-10}	8.694×10^{-7}	1.682×10^{-4}
8	0.75h	1.741×10^{-9}	8.689×10^{-7}	1.681×10^{-4}
7	0.65h	2.967×10^{-9}	8.665×10^{-7}	1.677×10^{-4}
6	0.55h	5.622×10^{-9}	8.618×10^{-7}	1.668×10^{-4}
5	0.45h	1.136×10^{-8}	8.537×10^{-7}	1.652×10^{-4}
4	0.35h	2.439×10^{-8}	8.352×10^{-7}	1.616×10^{-4}
3	0.25h	5.421×10^{-8}	7.961×10^{-7}	1.540×10^{-4}
2	0.15h	1.581×10^{-7}	6.900×10^{-7}	1.335×10^{-4}
1	0.05h	6.110×10^{-7}	3.055×10^{-7}	5.911×10^{-5}

$(h\bar{u})_d = 1.513 \times 10^{-3}$

$(h\bar{u})_e = 1.728 \times 10^{-3}$

$[(h\bar{u})_e - (h\bar{u})_d]/(h\bar{u})_d = 14.2\%$

internally as is supplied to the ice sheet by normal geothermal flux (Paterson, 1981, p.201). Depth-averaged balance velocity is about $28ma^{-1}$ at a point 715 km from Dome C. Thus, ignoring internal heat of deformation should significantly understate deformational velocities.

Published estimates of basal sliding downglacier from Dome C are scarce. Hughes and others (1981) postulate a basal freezing zone downglacier from Dome C, where basal sliding should be slow to zero. Budd and others (1971) show flowlines from Dome C to the coast to be almost entirely frozen to the bed.

In conclusion, bottom sliding might account for 30 percent or more of total ice flux, or the ice sheet may be frozen to the bed and not sliding in most regions. It appears most likely that bottom sliding occurs but is minor, and that taking bottom sliding to be identically zero is a reasonable assumption.

Appendix E. Initial estimates of depth-averaged longitudinal-deviatoric stress.

Solution of the flow model developed in this study requires initial estimates of depth-averaged longitudinal-deviatoric stress, $\bar{\sigma}'_x$, which are adjusted using an iterative technique. Two different methods for calculation of initial values of $\bar{\sigma}'_x$ have been tried: a simplified flow model and substitution of typical values into equation (13). Both methods give similar results.

Ei. Simplified flow model.

The approach adopted here is to calculate balance ice fluxes for an ice sheet frozen to its bed with no longitudinal-deviatoric stresses, and then calculate the longitudinal-deviatoric stresses that these fluxes would cause. For $\bar{\sigma}'_x=0$, the flow law reduces to

$$\frac{\partial u}{\partial z}=2A\tau_{xz}^{3} \tag{E1}$$

Substituting for τ_{xz} from equation (3) and integrating over depth yields

$$u=2A(\rho g\frac{\partial h}{\partial x})^3(h^3z-\frac{3}{2}h^2z^2+hz^3-\frac{1}{4}z^4) \tag{E2}$$

Taking the flow-law parameter to be a weighted average over depth and integrating (E2) over thickness then yields

$$(h\bar{u})=\frac{2}{5}\bar{A}(\rho g\frac{\partial h}{\partial x})^3h^5 \tag{E3}$$

and taking the derivative with respect to x

$$\frac{\partial(h\bar{u})}{\partial x}=2\bar{A}(\rho g)^3(h\frac{\partial h}{\partial x})^4+\frac{6}{5}\bar{A}(\rho g)^3h^5(\frac{\partial h}{\partial x})^2\frac{\partial^2 h}{\partial x^2} \tag{E4}$$

Next, it is assumed that longitudinal-deviatoric stresses do exist, and can be replaced by weighted averages over depth. Then, integrating the longitudinal flow law (1) through thickness and substituting for u(h) from (E2) yields

$$\frac{\partial}{\partial x}(h\bar{u})=\bar{A}\int_o^h\{\bar{\sigma}'^3_x+[\rho g(h-z)\frac{h}{x}]^2\bar{\sigma}'_x\}dz+\frac{1}{2}\bar{A}(\rho g)^3(h\frac{\partial h}{\partial x})^4 \tag{E5}$$

Equating (E4) and (E5) and simplifying then yields

$$\int_o^h \{\bar{\sigma}'^3_x + [\rho g(h-z)\frac{\partial h}{\partial x}]^2 \bar{\sigma}'_x\} dz = (\rho g)^3 h^4 (\frac{\partial h}{\partial x})^2 [\frac{3}{2}(\frac{\partial h}{\partial x})^2 + \frac{6}{5} h \frac{\partial^2 h}{\partial x^2}] \quad \text{(E6)}$$

Next, it is assumed that shear stress is much larger than longitudinal-deviatoric stress; that is,

$$\rho g(h-z)\frac{\partial h}{\partial x} > \bar{\sigma}'_x \quad \text{(E7)}$$

and (E6) becomes

$$\int_o^h (h-z)^2 \bar{\sigma}'_x dz = \rho g h^4 [\frac{3}{2}(\frac{\partial h}{\partial x})^2 + \frac{6}{5} h \frac{\partial^2 h}{\partial x^2}] \quad \text{(E8)}$$

The integral equation (E8) is satisfied for

$$\bar{\sigma}'_x = 18\rho g[(\frac{\partial h}{\partial x})^2 z + 2\frac{\partial^2 h}{\partial x^2} z^2] \quad \text{(E9)}$$

Integrating (E9) through thickness,

$$\bar{\sigma}'_x = \rho g h[9(\frac{\partial h}{\partial x})^2 + 12 h \frac{\partial^2 h}{\partial x^2}] \quad \text{(E10)}$$

Initial estimates of $\bar{\sigma}'_x$ can then be calculated from ice-sheet configuration using (E10).

Eii. Substitution of typical values into equation (13).

Equation (13) is an implicit statement of $\bar{\sigma}'_x$ in terms of ice-sheet configuration. Approximate values of parameters involved in equation (13) for East Antarctica are listed in table EI. Typical values of both $\bar{\sigma}'_x$ and its derivative with respect to x can be calculated using methods in appendices B-D, or using equation (E10). Values of each term in equation (13), calculated using numbers from table EI, are listed in table EII.

From table EII, it is evident that equation (13) may be approximated by

$$0=\frac{1}{3}(\rho gh\frac{\partial h}{\partial x})^2\bar{\sigma}'_x-\frac{3}{2}(\rho gh)^3(\frac{\partial h}{\partial x})^4-\frac{6}{5}(\rho g)^3h^4(\frac{\partial h}{\partial x})^2\frac{\partial^2 h}{\partial x^2} \qquad \text{(E11)}$$

which can be solved for $\bar{\sigma}'_x$ to give

$$\bar{\sigma}'_x=\rho gh[\frac{9}{2}(\frac{\partial h}{\partial x})^2+\frac{18}{5}h\frac{\partial^2 h}{\partial x^2}] \qquad \text{(E12)}$$

which differs from (E10) only by constants. Equation (E12) was used in this study.

Table EI. Typical values of parameters for East Antarctica.

All units mks.

ρ	910
g	-9.8
h	$3\times10^{+3}$
$\frac{\partial h}{\partial x}$	-2×10^{-3}
$\frac{\partial^2 h}{\partial x^2}$	-5×10^{-9}
$\bar{\sigma}'_x$	10^{+3}
$\frac{\partial \bar{\sigma}'_x}{\partial x}$	$\pm2\times10^{-3}$
u_b	$0.00\times10^{+0}$

Table EII. Calculated terms in equation (13), using numbers from table (EI). All units mks.

$\bar{\sigma}'_x$	$1.0\times10^{+9}$
$-\rho gh(\frac{\partial h}{\partial x})^2 \bar{-}'_x$	$1.1\times10^{+8}$
$-\frac{2}{3}\rho gh^2\frac{\partial^2 h}{\partial x^2}\bar{\sigma}'_x$	$-2.7\times10^{+8}$
$\frac{1}{3}(\rho gh\frac{\partial h}{\partial x})^2 \bar{-}'_x$	$9.5\times10^{+11}$
$-\frac{4}{3}\rho gh^2\frac{\partial h}{\partial x}\frac{\partial \bar{\sigma}'_x}{\partial x}$	$\pm4.3\times10^{+8}$
$-\frac{3}{2}(\rho gh)^3(\frac{\partial h}{\partial x})^4$	$4.6\times10^{+11}$
$-\frac{6}{5}(\rho g)^3(\frac{\partial h}{\partial x})^2\frac{\partial^2 h}{\partial x^2}h^4$	$-1.4\times10^{+12}$
$u_b\frac{\partial h}{\partial x}$	$0.00\times10^{+0}$

Appendix F. Response times of ice sheets with terminal positions controlled by sea level compared to response times of ice sheets free to advance or retreat.

An increase in accumulation rate causes an ice sheet to thicken to a new equilibrium configuration. This response has been modelled by Nye (1960), Whillans (1981), and Bolzan (class II, n=2; 1984) using the form

$$\Delta h = \theta \Delta \dot{b} [1 - \exp(-\frac{t}{\theta})] \qquad \text{(F1)}$$

where t is time, h is change in ice-sheet thickness from original thickness h, $\dot{b}$ is change in accumulation rate from the initial value $\dot{b}$, and is the response time given by

$$\theta = \frac{h}{(p+2)\dot{b}} \qquad \text{(F2)}$$

where p is a constant (Nye, 1960, near an ice divide; Whillans, 1981; Bolzan, 1984, class II, n=2, near an ice divide). The constant p is equal to one in the Nye (1960), Whillans, and Bolzan models. The Nye (1960) model assumed that all motion is by basal sliding, and that no diffusion of kinematic waves occurs. In later models he allowed for internal deformation, which increased p to between one and four, and for diffusion, which decreased p back toward one (a good summary of the Nye models is given in Paterson, 1981, p.241-267).

The (F1)-type models use the assumption that thickness changes, but that surface slope does not change. This may be a good approximation for an ice sheet that is free to advance when

accumulation rate increases, although it is probably strictly true only rarely. This assumption is generally not valid for an ice sheet with terminal position controlled by sea level. In such an ice sheet, increase in thickness increases surface slope except at the ice divide. Because the ice sheet responds smoothly, response at the ice divide also will reflect control of the terminal position by sea level, even though surface slope does not change there.

To assess the importance of this increase in surface slope to ice-sheet response, consider a simplified ice sheet with no longitudinal stresses. Integrating the flow law through thickness twice, expressing in terms of the horizontal gradient in horizontal ice flux, and combining with the continuity relation (4) gives

$$\dot{h}=\dot{b}-\bar{A}(\rho g)^3\left[2\left(h\frac{\partial h}{\partial x}\right)^4+\frac{6}{5}h^5\left(\frac{\partial h}{\partial x}\right)^2\frac{\partial^2 h}{\partial x^2}\right] \qquad \text{(F3)}$$

The two terms enclosed within square brackets are of the same order of magnitude.

If the ice-sheet surface were a straight line from the ice divide to the terminus, then percentage changes in h and $(\frac{\partial h}{\partial x})$ would be equal, and their effect on the time-rate of change of thickness would be equal. In such an ice sheet, the assumption that surface slope remains constant would lead to serious errors in calculated response.

For a 10 percent increase in accumulation rate from modern values at Dome C, the model (F1) and (F2), with p equal to one, predicts

40.2 m thickening after 15,000 years, steady-state thickening of 106.1 m, and a response time of about 31,500 years. The response model developed in this paper calculates a thickening of 34.1 m, with steady-state thickening of 39.0 m. The model developed here does not respond according to (F1). Fitting (F1) to thickening calculated here for 15,000 years gives steady-state thickening of 51.8 m, a response time of 14,000 years, and the constant p equal to 4.8. Fitting (F1) to steady-state thickening calculated here gives thickening of 29.6 m after 15,000 years, response time of 10,500 years, and the constant p equal to 7.0. In either case, it is evident that when subjected to an increase in accumulation rate, an ice sheet with terminal position controlled by sea level responds more rapidly and has less total response than an ice sheet free to advance, although differences are not large for the first 15,000 years.

Temperature increase softens ice and causes inland-ice-sheet thinning. Such response has been modelled for shear-dominated accumulation zones, assuming that surface slope does not change (Whillans, 1981). For fixed terminal position, thinning will decrease the surface slope, which will decrease the rate of thinning, the response time, and total change in thickness to new equilibrium.

It is clear, then, that the inland response of an ice sheet to changes in accumulation rate or temperature depends on conditions at the terminus. If the terminus is free to advance or retreat, then response times are long and total change in thickness is large. If the position of the terminus is controlled by sea level, then response

times are shorter and total change in thickness is smaller, assuming that the ice sheet responds in a stable manner and approaches a new equilibrium. On a time scale of one response time of an ice sheet with controlled terminus, however, differences between the two types of models are not large.

Appendix G. Listing of FORTRAN computer program for model with longitudinal-deviatoric stress.

```
C  glacier.fort
      implicit real*8(A-H,O-Z)
      common nxvalu,nextrp,none,nxone,xstep,rhog,rh,dh,d2h,sigma,dsigma,
     #ra,df,tstep,delsig,rbdot
      dimension rh(21),dh(21),d2h(21),sigma(21),dsigma(21),delsig(21),
     #bdot(21),rbdot(21),ra(21),df(21)
C  all arrays are dimensioned to the number of grid points, here 21
C  choose (start-end) to be an even multiple of the number of grid
C   points minus one.
C  rh holds ice-sheet thickness, dh holds first spatial derivative of
C   rh, and d2h holds second spatial derivative.  sigma holds
C   longitudinal-deviatoric stresses, and dsigma the derivatives of
C   sigma.  delsig is used to adjust sigma in iterative solution
C   for sigma.
      Data a/5.d-25/,rho/910./,g/-9.8/,rhmax/3600./,xmax/9.3d5/,pass/0./
     #,start/0.5d5/,end/8.0d5/,time/1.5d4/delbdt/1.2/,finend/1342.38/,tt
     #hin/1.0d4/
C  a is initial estimate of flow-law parameter, ra is calculated steady
C   value of a
C  rho is density of ice
C  g is acceleration of gravity
C  rhmax is thickness at the ice divide
C  xmax is half-width of the ice sheet
C  nxvalu is number of grid points
C  start is x coordinate for beginning of calculations
C  end is x coordinate for end of calculations
C  finend is final thickness at end point
C  tthin is time for sea level to rise
      nxvalu=21
      none=1
      nxone=nxvalu-1
      tstep=1
      ntstep=time/tstep
      xstep=(end-start)/nxone
      nextrp=10
      nxalso=nxvalu
      nlalso=none
      rhog=rho*g
C  print out heading
      perdbd=(delbdt-1.0)*100.
      write (6,600)
      write (6,601) tstep,time,tthin
      write (6,602) start,end,perdbd
      write (6,603) xmax,rhmax
C  nxvalu and nxalso are number of grid points, nlalso and none are one,
C   nxone is one less than the number of grid points,
```

```
C  nextrp is the number of points used in fitting a curve to estimate
C   slopes at end points
C  tstep is the number of years in each time step, nstep is the
C   total number of time steps in the run, which lasts for time years
C  xstep is the length of distance steps
C
C  Generate initial thickness and its derivatives,
C   and guess initial longitudinal-deviatoric stresses
C  Run from start to end km from ice divide
C  x is horizontal position
      do 2 i=1,nxvalu
      x=start+(i-1)*xstep
C  rbdot is analytic fit to measured accumulation rates, which is
C   adjusted to Wisconsinan-maximum values by delbdt.
      rbdot(i)=5.4138d-3*dexp(4.6954d-6*x)+3.4586d-2
      rbdot(i)=rbdot(i)/delbdt
C  ice thickness is calculated according to the vialov profile
    2 rh(i)=rhmax*(1.-(x/xmax)**(4./3.))**(3./8.)
C  drhend is the amount that the terminal grid point thins per time step
      drhend=tstep*(rh(nxvalu)-finend)/tthin
      call dervrh (nlalso,nxalso)
C
C  Make initial guess at longitudinal-deviatoric stresses and then
C   adjust iteratively to actual values
      do 13 i=1,nxvalu
   13 sigma(i)=9./2.*rhog*rh(i)*dh(i)**2+18./5.*rhog*rh(i)**2*d2h(i)
      call dervsg(nlalso,nxalso)
      call solvsg(nlalso,nxalso)
C  write steady-state values of parameters
      write (6,400)
      write(6,500)(k,rh(k),dh(k),d2h(k),sigma(k),dsigma(k),k=1,nxvalu,4)
C  calculate steady-state values of the flow-law parameter
C  the numerical factor 3.16d7 converts accumulation rate per year to
C   accumulation rate per second
      do 20 i=1,nxvalu
      s=sigma(i)
      b=rhog*rh(i)*dh(i)
      stress=rh(i)*(s**3+b*dh(i)*s**2+1./3.*b**2*s+.5*b**3*dh(i))*3.16d7
   20 ra(i)=rbdot(i)/stress
      write (6,396)
      write (6,300)(ra(i),i=1,nxvalu)
C
C  change accumulation rate to modern values.  df(i) is horizontal
C   gradient in ice flux.
      do 70 i=1,nxvalu
      df(i)=rbdot(i)
   70 rbdot(i)=delbdt*rbdot(i)
C
C  set up loop for time stepping
      do 51 m=1,ntstep
```

```
      call contnu(nlalso,nxalso)
C  thin end if sea level is still rising
      ttt=tthin/ntstep
      if (m.le.ttt) rh(nxvalu)=rh(nxvalu)-drhend
      call solvsg (nlalso,nxalso)
      call flolaw
C
C  write results every 100a for first 500a, then every 500a for next
C   1500a, then every 1000a for rest of run
      mmm=100
      if (m.gt.500) mmm=500
      if (m.gt.2000) mmm=1000
      if (mmm*(m/mmm).ne.m) go to 51
      t=m*tstep
      write (6,190)
      write (6,420) t
      write (6,190)
      write (6,400)
      write(6,500)(k,rh(k),dh(k),d2h(k),sigma(k),dsigma(k),k=1,nxvalu,4)
   51 continue
   52 continue
      stop
  190 format (' ')
  300 format (' ',7e13.4)
  396 format ('0',/' ra(i)')
  400 format('0',/'   i      rh(i)        dh(i)       d2h(i)          si
     #gma(i)     dsigma(i)  ')
  420 format ('0',/' time=',e13.4)
  500 format ('0',i3,5e14.5)
  600 format ('0','no longitudinal stress model, east antarctica')
  601 format ('0','tstep=',f5.2,' time=',f8.2,' new thick. at end in ',f
     #8.2,' years')
  602 format ('0','start=',d10.3,'km., end=',d10.3,'km., ',f6.2,
     #'% change in bdot')
  603 format ('0','xmax=',d10.3,'km., rhmax=',d11.4,' at t=0, 850 km. fo
     #r tgt0')
      end
C
C**********************************************************************
C  extrap calculates first and second derivatives of array y at point ix
C   which may be nlalso or nxalso
C  a holds coefficients to polynomial fit to nextrp points of y
C  z holds end point and extrapolated and interpolated points that
C   have spacing xsi.  y must be of dimension nxvalu, and a must be of
C   dimension nextrp.
      subroutine extrap (ix,iy)
      implicit real*8(a-h,o-z)
      dimension rh(21),dh(21),d2h(21),sigma(21),dsigma(21),delsig(21),
     #bdot(21),rbdot(21),ra(21),df(21),a(10),z(3)
```

```
      common nxvalu,nextrp,none,nxone,xstep,rhog,rh,dh,d2h,sigma,dsigma,
     #ra,df,tstep,delsig,rbdot
      percen=0.02
      xsi=xstep*percen
      if (iy.eq.1) z(2)=rh(ix)
      if (iy.eq.2) z(2)=sigma(ix)
      do 1 j=1,nextrp
      a(j)=0.
      do 2 i=1,j
      if (ix.eq.none) m=1
      if (ix.eq.nxvalu) m=nxvalu+1-i
      k=i-1
      n=j-i
      if (iy.eq.1) y=rh(m)
      if (iy.eq.2) y=sigma(m)
    2 a(j)=a(j)+(-1)**n*y/(nfact(k)*nfact(n))
    1 continue
      do 8 ii=1,3,2
      sum=a(1)
      delta=(2-ii)*percen
      do 3 j=2,nextrp
      prod=1.
      jminus=j-1
      do 4 i=1,jminus
    4 prod=prod*(delta-i+1)
    3 sum=sum+a(j)*prod
    8 z(ii)=sum
      d1=(z(1)-z(3))/(2.*xsi)
      if (ix.eq.nxvalu) d1=(-1.)*d1
      d2=(z(1)-2.*z(2)+z(3))/xsi**2
      if (iy.eq.1) dh(ix)=d1
      if (iy.eq.1) d2h(ix)=d2
      if (iy.eq.2) dsigma(ix)=d1
      return
      end
C
C ***************************************************************************
C  nfact calculates the factorial of an integral number
C  if (number.lt.2),nfact(number)=1 by definition
      function nfact(number)
      iaccum=1
      if (number.lt.2) go to 7
      do 6 n=2,number
      iaccum=iaccum*n
    6 continue
    7 continue
      nfact=iaccum
      return
      end
```

```
C
C**********************************************************************
C  dervrh calculates first and second derivatives with x for
C   all points in rh.
      subroutine dervrh (nlalso,nxalso)
      implicit real*8(a-h,o-z)
      dimension rh(21),dh(21),d2h(21),sigma(21),dsigma(21),delsig(21),
     #bdot(21),rbdot(21),ra(21),df(21),a(10),z(3)
      common nxvalu,nextrp,none,nxone,xstep,rhog,rh,dh,d2h,sigma,dsigma,
     #ra,df,tstep,delsig,rbdot
      do 12 i=2,nxone
      dh(i)=(rh(i+1)-rh(i-1))/(2.*xstep)
   12 d2h(i)=(rh(i+1)-2.*rh(i)+rh(i-1))/xstep**2
      call extrap (nlalso,1)
      call extrap (nxalso,1)
      return
      end
C
C**********************************************************************
C  dervsg calculates first space derivatives for all points in sigma
      subroutine dervsg (nlalso,nxalso)
      implicit real*8(a-h,o-z)
      dimension rh(21),dh(21),d2h(21),sigma(21),dsigma(21),delsig(21),
     #bdot(21),rbdot(21),ra(21),df(21),a(10),z(3)
      common nxvalu,nextrp,none,nxone,xstep,rhog,rh,dh,d2h,sigma,dsigma,
     #ra,df,tstep,delsig,rbdot
      do 3 j=2,nxone
    3 dsigma(j)=(sigma(j+1)-sigma(j-1))/(2.*xstep)
      call extrap (nlalso,2)
      call extrap (nxalso,2)
      return
      end
C
C**********************************************************************
C  solvsg calculates longitudinal stress deviators in equilibrium
C   with a given ice-sheet configuration
      implicit real*8(a-h,o-z)
      dimension rh(21),dh(21),d2h(21),sigma(21),dsigma(21),delsig(21),
     #bdot(21),rbdot(21),ra(21),df(21),a(10),z(3)
      common nxvalu,nextrp,none,nxone,xstep,rhog,rh,dh,d2h,sigma,dsigma,
     #ra,df,tstep,delsig,rbdot
      icount=0
    5 do 10 i=1,nxvalu
C  calculate constants to calculate changes in sigma
      a2=rhog*rh(i)*dh(i)**2+2./3.*rhog*rh(i)**2*d2h(i)
      a3=1./3.*(rhog*rh(i)*dh(i))**2-4./3.*rhog*rh(i)**2*dh(i)*dsigma(i)
      aa=1.5*(rhog*rh(i))**3*dh(i)**4
      ab=1.2*rhog**3*rh(i)**4*dh(i)**2*d2h(i)
      a4=aa+ab
      delsl=sigma(i)**3-a2*sigma(i)**2+a3*sigma(i)-a4
```

```
      dels2=-3.*sigma(i)**2+2.*a2*sigma(i)-a3
      delsig(i)=delsl/dels2
C  set up check for convergence
C   percng is percentage change in sigma
      percng=dabs(delsig(i)/sigma(i))
C  for each grid pt. that changes less than 0.01% increase icount by 1
      if (percng.lt.0.0001) icount=icount+1
   10 sigma(i)=delsig(i)+sigma(i)
C  calculate new space derivatives of sigma
      call dervsg (nlalso,nxalso)
C  if some grid point changed more than 0.01% in sigma,
C   repeat loop to adjust sigma
      if (icount.lt.nxvalu) icount=0
      if (icount.eq.0) go to 5
      return
      end
C
C*********************************************************************
C  flolaw calculates ice fluxes for given sigma, ice-sheet
C   configuration, and constants
      subroutine flolaw
      implicit real*8(a-h,o-z)
      dimension rh(21),dh(21),d2h(21),sigma(21),dsigma(21),delsig(21),
     #bdot(21),rbdot(21),ra(21),df(21),a(10),z(3)
      common nxvalu,nextrp,none,nxone,xstep,rhog,rh,dh,d2h,sigma,dsigma,
     #ra,df,tstep,delsig,rbdot
C  correct sigma are known, so plug into flow law
      do 20 i=1,nxvalu
      s=sigma(i)
      b=rhog*rh(i)*dh(i)
      df(i)=ra(i)*rh(i)*(s**3+b*dh(i)*s**2+1./3.*b**2*s+.5*b**3*dh(i))*3
     #.16d7
   20 continue
      return
      end
C
C*********************************************************************
C  contnu calculates change in thickness and new thickness for
C   given fluxes and accumulations
      subroutine contnu (nlalso,nxalso)
      implicit real*8(a-h,o-z)
      dimension rh(21),dh(21),d2h(21),sigma(21),dsigma(21),delsig(21),
     #bdot(21),rbdot(21),ra(21),df(21),a(10),z(3)
      common nxvalu,nextrp,none,nxone,xstep,rhog,rh,dh,d2h,sigma,dsigma,
     #ra,df,tstep,delsig,rbdot
      do 71 i=1,nxone
      rhdot=rbdot(i)-df(i)
   71 rh(i)=rh(i)+rhdot*tstep
      call dervrh (nlalso,nxalso)
      return
      end
```

Appendix H. Listing of FORTRAN computer program for model with no longitudinal-deviatoric stress.

```
c  program assumes no longitudinal stresses, ice divide fixed position
c  program similar to longitudinal stress model
c
c  initialize
      implicit real*8(a-h,o-z)
      common nxvalu,nxone,nxtwo,xstep,start1,rh,dh,d2h
      dimension rh(21),dh(21),d2h(21),rbdot(21),ra(21)
      data rho/910./,g/-9.8/,rhmax/3615./,xmax/9.3d5/,start/1.0d4/,end/8
     #0d5/,time/1.5d4/,delbdt/1.0/,tthin/1.0d4/,finend/1342.4/
      nxvalu=21
      nxone=nxvalu-1
      nxtwo=nxvalu-2
      tstep=1.
      ntstep=time/tstep
      start1=start
      xstep=(end-start)/nxone
c
c  print heading
      perdbd=(delbdt-1.0)*100.
      write (6,600)
      write (6,601) tstep,time,tthin
      write (6,602) start,end,perdbd
      write (6,603) xmax,rhmax
c
c  calculate and print initial steady-state values
      do 2 i=1,nxvalu
      x=start+(i-1)*xstep
      rbdot(i)=5.4138d-3*dexp(4.6954d-6*x)+3.1586d-2
      rbdot(i)=rbdot(i)/delbdt
    2 rh(i)=rhmax*(1.-(x/xmax)**(4./3.))**(3./8.)
      drhend=tstep*(rh(nxvalu)-finend)/tthin
      call dervrh
      do 20 i=1,nxvalu
      b=2.*(rho*g)**3*rh(i)**4*dh(i)**2
      bb=b*(3./5.*rh(i)*d2h(i)+dh(i)**2)*3.16d7
   20 ra(i)=rbdot(i)/bb
      write (6,400)
      write (6,500)(k,rh(k),dh(k),d2h(k),ra(k),k=1,nxvalu,4)
      do 70 i=1,nxvalu
   70 rbdot(i)=delbdt*rbdot(i)
c  time step
      do 51 m=1,ntstep
      ttplus=tthin+0.5
      if (m.lt.ttplus)rh(nxvalu)=rh(nxvalu)-drhend
      do 52 i=1,nxone
      rhdot=rbdot(i)-2*ra(i)*(rho*g)**3*rh(i)**4*dh(i)**2*(3./5.*rh(i)*
     #d2h(i)+dh(i)**2)*3.16d7
```

```
   52 rh(i)=rh(i)+rhdot*tstep
      call extrap
      call dervrh
c
c  print results of time-stepping
      mmm=100
      if (m.gt.500) mmm=500
      if (m.gt.2000)mmm=1000
      if (mmm*(m/mmm).ne.m) go to 51
      t=m*tstep
      write (6,190)
      write (6,420) t
      write (6,190)
      write (6,400)
      write (6,500)(k,rh(k),dh(k),d2h(k),ra(k),k=1,nxvalu,4)
   51 continue
      stop
  190 format (' ')
  400 format ('0',/'    i       rh(i)          dh(i)         d2h(i)
     #ra(i)')
  420 format ('0',/' time=',e13.4)
  500 format (' ',i3,4d14.5)
  600 format ('0','no longitudinal stress model, east antarctica')
  601 format ('0','tstep=',f5.2,' time=',f8.2,' new thick. at end in ',f
     #8.2,' years')
  602 format ('0','start=',d10.3,'km., end=',d10.3,'km., ',f6.2,
     #'% change in bdot')
  603 format ('0','xmax=',d10.3,'km., rhmax=',d11.4,' at t=0, 850 km. fo
     #r tgt0')
      end
C
C ***************************************************************************
      subroutine dervrh
      implicit real*8(a-h,o-z)
      common nxvalu,nxone,nxtwo,xstep,start1,rh,dh,d2h
      dimension rh(21),dh(21),d2h(21),rbdot(21),ra(21)
      start=start1
      do 12 i=2,nxone
      dh(i)=rh(i+1)-rh(i-1))/(2.*xstep)
   12 d2h(i)=(rh(i+1)-2.*rh(i)+rh(i-1))/xstep**2
      dh(1)=dh(2)*start/(xstep+start)
      d2h(i)=(dh(1)*xstep**2-start**2)+dh(2)*start**2)/(start*xstep*
     #(start+xstep))
      do 13 i=1,2
      if (i.eq.2) go to 14
      a1=rh(nxvalu)
      a2=rh(nxone)
      a3=rh(nxtwo)
      go to 15
   14 a1=dh(nxvalu)
```

```
      a2=dh(nxone)
      a3=dh(nxtwo)
   15 d1=(a1-a2)/xstep
      d2=(a2-a3)/xstep
      d3=d1-0.5*(d2-d1)
      if (i.eq.1) dh(nxvalu)=d3
      if (i.eq.2) d2h(nxvalu)=d3
   13 continue
      return
      end
C
C ***************************************************************************
      subroutine extrap
      implicit real*8(a-h,o-z)
      common nxvalu,nxone,nxtwo,xstep,start1,rh,dh,d2h
      dimension rh(21),dh(21),d2h(21),rbdot(21),ra(21),a(10)
      do 11 j=1,10
      a(j)=0.
      do 10 i=1,j
      k=nxvalu-i
      a(j)=a(j)+(-1.)**(j-i)*rh(k)/(nfact(i-1)*nfact(j-i))
   10 continue
   11 continue
      rh(nxvalu)=a(1)
      do 12 j=2,10
      prod=1.
      m=j-1
      do 13 i=1,m
   13 prod=prod*i*(-1)
      prod=prod*a(j)
   12 rh(nxvalu)=rh(nxvalu)+prod
      return
      end
C
C ***************************************************************************
C  nfact calculates the factorial of an integral number
C  if (number.lt.2),nfact(number)=1 by definition
      function nfact(number)
      iaccum=1
      if (number.lt.2) go to 7
      do 6 n=2,number
      iaccum=iaccum*n
    6 continue
    7 continue
      nfact=iaccum
      return
      end
```

REFERENCES

Blankenship, D.D. (1982) P-wave anisotropy in the high polar ice of East Antarctica. M.Sc. Thesis, University of Wisconsin-Madison, 143p.

Bloom, A.L., W.S. Broecker, J.M.A. Chappell, R.K. Matthews, and K.J. Mesolella (1974) Quaternary sea-level fluctuations on a tectonic coast: New 230Th/234U dates from the Huon Peninsula, New Guinea: Quaternary Research, v. 4, p. 185-205.

Bolzan, J.F., (1984) Ice dynamics at Dome C, East Antarctica: Ohio State Univ. Inst. Polar Stud. Rept. No. 85, 55p.

Budd, W.F. (1968) The longitudinal velocity profile of large ice masses. International Association of Scientific Hydrology Publication No. 79, p. 58-75.

Budd, W.F. (1970) Ice flow over bedrock perturbations. Journal of Glaciology, v. 9, p. 29-48.

Budd, W.F., D. Jenssen, and U. Radok (1971) Derived physical characteristics of the Antarctic ice sheet. University of Melbourne Meteorology Department Publication No. 18, 178p.

Bull, C. (1971) Snow accumulation in Antarctica: p. 367-421 In Quam, L.O., ed., Research in the Antarctic, American Association for the Advancement of Science, Washington, D.C.

Cameron, R.L. and R.P. Goldthwait (1961) The U.S.-I.G.Y. contribution to Antarctic glaciology: International Association of Scientific Hydrology Publication No. 55, p.7-13.

Clarke, G.K.C., U. Nitsan, and W.S.B. Paterson (1977) Strain heating and instability in glaciers and ice sheets: Reviews of Geophysics and Space Physics, v. 15, p. 235-247.

Drewry, D.J. (1982) Antarctica unveiled: New Scientist, 22 July 1982, p. 246-251.

Fairbridge, R.W. (1961) Eustatic changes in sea level. p. 99-185 In Ahrens, L.H., ed., Physics and Chemistry of the Earth 4, Pergamon Press, London.

Hollin, J.T. (1962) On the glacial history of Antarctica. Journal of Glaciology, v. 4, p. 173-195.

Hooke, R.LeB. (1981) Flow law for polycrystalline ice in glaciers: Comparison of theoretical predictions, laboratory data, and field measurements: Reviews of Geophysics and Space Physics, v. 19, p. 664-672.

Hooke, R.LeB. and P.J. Hudleston (1980) Ice fabrics in a vertical flow plane, Barnes Ice Cap, Canada: Journal of Glaciology, v. 25, p. 195-214.

Hughes, T.J., D.H. Denton, B.G. Anderson, D.H. Schilling, J.L Fastook, and C.S. Lingle (1981) The last great ice sheets: A global view: p. 275-318 In Hughes, T.J. and D.H. Denton, eds., The Last Great Ice Sheets, Wiley and Sons, New York.

Jankowski, E.J. and D.J. Drewry (1981) The structure of West Antarctica from geophysical studies: Nature, v. 291, p. 17-21.

Kamb, B. (1970) Sliding motion of glaciers: Theory and observation: Reviews of Geophysics and Space Physics. v. 8, p. 673-728.

Lliboutry, L. (1975) Loi de glissement d'un glacier sans cavitation: Annales de Gèophysique, v. 31, p. 207-226.

Lorius, C., D. Raynaud, J.R. Petit, J. Jouzel, and L Merlivat (1984) Late Glacial Maximum-Holocene atmospheric and ice thickness changes from Antarctic ice core studies. Annals of Glaciology, v. 5.

Mahaffy, M.W. (1976) A three-dimensional numerical model of ice sheets: Tests on the Barnes Ice Cap, Northwest Territories: Journal of Geophysical Research, v. 81, p. 1059-1066.

Meguro, H., Y. Yoshida, T. Uchio, K. Kigoshi, and K. Sugawara (1963) Quaternary marine sediments and their geological dates with reference to the geomorphology of the Kronprins Olav Kyst: Antarctic Geology, Scientific Committee on Antarctic Research Proceedings, p. 73-79.

Mercer, J.H. (1968) Glacial geology of the Reedy Glacier area, Antarctica: Geological Society of America Bulletin, v. 79, p. 471-486.

Mercer, J.H. (1972) Some observations on the glacial geology of the Beardmore Glacier area: p. 427-433 In, Adie, R.J., ed., Antarctic Geology and Geophysics, Universitetsforlaget, Oslo.

Milliman, J.D. and K.O. Emery (1968) Sea levels during the past 35,000 years: Science, v. 162, p. 1121-1123.

Mörner, N-A (1971) The position of the ocean level during the interstadial at about 30,000 B.P.-A discussion from a climatic-glaciologic point of view: Canadian Journal of Earth Sciences, v. 8, p. 132-143.

Nye, J.F. (1959) The motion of ice sheets and glaciers: Journal of Glaciology, v. 3, p. 493-506.

Nye, J.F. (1960) The response of glaciers and ice-sheets to seasonal and climatic changes. Proceedings of the Royal Society of London, Series A, v. 256, p. 559-584.

Nye, J.F. (1969) A calculation of the sliding of ice over a wavy surface using a Newtonian viscous approximation. Proceedings of the Royal Society of London, Series A, v. 311, p. 445-467.

Nye, J.F. (1970) Glacier sliding without cavitation in a linear viscous approximation. Proceedings of the Royal Society of London, Series A, v. 315, p. 381-403.

Oswald, G.K.A. and G. de Q. Robin (1973) Lakes beneath the Antarctic ice sheet: Nature, v. 245, p. 251-254.

Paterson, W.S.B. (1976) Vertical strain-rate measurements in an arctic ice cap and deductions from them: Journal of Glaciology, v. 17, p. 3-12.

Paterson, W.S.B. (1981) The Physics of Glaciers, Second Edition. Pergamon Press, Oxford, 380p.

Raynaud, D. (1976) Les inclusions gazeuses dans la glace de glacier; leur utilisation comme indicatuer du site de formation de la glace polaire; applications climatiques et rheologiques, These de Doctorat d'etat, Universite Scientifique et Medicale de Grenoble. Publication No. 214 of the Laboratory of Geology, Centre National de la Recherche Scientifiques, 111p.

Robin, G. de Q. (1955) Ice movement and temperature distribution in glaciers and ice sheets: Journal of Glaciology, v. 2, p. 523-532.

Robin, G. de Q. (1977) Ice cores and climatic change: Philosophical Transactions of the Royal Society of London, Series B, v. 280, p. 143-168.

Shepard, F.P. (1963) Thirty-five thousand years of sea level: p. 1-10 In, Clements, T., ed., Essays in Marine Geology in Honor of K.O. Emery, University of Southern California Press, Los Angeles.

Stuiver, M., G.H. Denton, T.J. Hughes, and J.L. Fastook (1981) History of the marine ice sheet in West Antarctica during the last glaciation: A working hypothesis: p. 319-430 In Hughes, T.J. and D.H. Denton, ed., The Last Great Ice Sheets, Wiley and Sons, New York.

Thomas, R.H. (1973) The creep of ice shelves: Interpretation of observed behavior: Journal of Glaciology, v. 12, p. 55-70.

Thomas, R.H. (1977) Calving-bay dynamics and ice-sheet retreat up the St. Lawrence valley system: Geographie Physique Quaternaire, v. 31, p. 347-356.

Thomas, R.H. and C.R. Bentley (1978) A model for Holocene retreat of the West Antarctic ice sheet: Quaternary Research, v. 10, p. 150-170.

Thompson, L.G., E. Mosley-Thompson, and J.R. Petit (1981) Glaciological interpretation of microparticle concentrations from the French 905-m Dome C, Antarctica core. International Association of Scientific Hydrology Publication No. 131, p. 227-234.

Vialov, S.S. (1958) Regularities of glacial shields movement and the theory of plastic viscous flow. International Association of Scientific Hydrology Publication No. 47, p. 266-275.

Weertman, J. (1957) On the sliding of glaciers: Journal of Glaciology, v. 3, p. 33-38.

Weertman, J. (1964) The theory of glacier sliding: Journal of Glaciology, v. 5, p. 287-303.

Weertman, J. and G.E. Birchfield (1981) Subglacial water flow under ice streams and West Antarctic ice-sheet stability: Annals of Glaciology, v. 3, p. 316-320.

Whillans, I.M. (1981) Reaction of the accumulation zone portions of glaciers to climatic change: Journal of Geophysical Research, v. 86, p. 4274-4282.